Maximizing the use of aquifer thermal energy storage systems in urban areas effects on individual system primary energy use and overall GHG emissions

Beernink, Stijn; Bloemendal, Martin; Kleinlugtenbelt, Rob; Hartog, Niels

DOI
10.1016/j.apenergy.2022.118587

Publication date
2022

Document Version
Final published version

Published in
Applied Energy

Applied Energy 311 (2022) 118587

Contents lists available at ScienceDirect

Applied Energy

journal homepage: www.elsevier.com/locate/apenergy

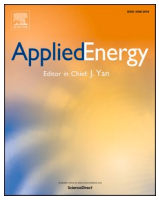

Maximizing the use of aquifer thermal energy storage systems in urban areas: effects on individual system primary energy use and overall GHG emissions

Stijn Beernink [a,b], Martin Bloemendal [a,b,*], Rob Kleinlugtenbelt [c], Niels Hartog [a]

[a] KWR Water Research Institute, Nieuwegein, the Netherlands
[b] Delft University of Technology, the Netherlands
[c] IF Technology, the Netherlands

HIGHLIGHTS

- The primary energy use of ATES systems evaluated for high and low aquifer utilisation levels.
- High aquifer utilisation levels reduce energy use of individual systems, as more wells can be placed.
- The highest aquifer utilization level considered is 115% and resulted in 82% ATES adoption.
- For aquifer utilization <80%, energy use of buildings is not affected by subsurface interactions.
- For aquifer utilization >80%, interactions affect gas use +15% and electricity use +/-15%.

ARTICLE INFO

Keywords:
Aquifer Thermal Energy Storage (ATES)
Subsurface interaction between ATES systems
Individual ATES system performance
Optimal utilisation of subsurface space

ABSTRACT

Low temperature (<25 °C) Aquifer Thermal Energy Storage (ATES) systems have a world-wide potential to provide low-carbon space heating and cooling for buildings by using heat pumps combined with the seasonal subsurface storage and recovery of heated and cooled groundwater. ATES systems increasingly utilize aquifer space, decreasing the overall primary energy use for heating and cooling for an urban area. However, subsurface interaction may negatively affect the energy performance of individual buildings with existing ATES systems. In this study, it is investigated how aquifer utilization levels, obtained by varying well placement policies, affect subsurface interaction between ATES systems and how this in turn affects individual primary energy use. To this end, a building climate installation model is developed and integrated with a MODFLOW-MT3DMS thermal groundwater model. For the spatial distribution and thermal requirements of 26 unique buildings as present in the city centre of Utrecht, the placement of ATES wells is varied using an agent-based modelling approach applying dense and spacious placement restrictions. Within these simulations ATES adoption order and well placement location is randomized. Well placement density is varied for 9 scenarios by changing the distance between wells of the same and the opposite type. The results of this study show that the applied dense well placement policies lead to a 30% increase of ATES adoption and hence overall GHG emission reduction improved with maximum 60% compared to conventional heating and cooling. The primary energy use of individual ATES systems is affected at varying well placement policies by two mechanisms. Firstly, at denser well placement, ATES systems are able to place more wells, which increases the capacity of their ATES system, thereby decreasing their electricity and gas use. Secondly, aquifer utilization increases with denser well placement policies and thus interaction between individual ATES increases. At subsurface utilization up to 80%, individual primary energy use does not change significantly due to subsurface interaction. At aquifer utilization level > 80%, both negative and positive interaction is observed. Negative interaction between wells of the opposite type leads to an increase of gas or electricity use up to 15% compared to spacious well placement. On the other side, buildings may experience a maximum decrease of 15% electricity use at dense well placement due to positive interaction between wells of the same type. Local conditions like building location, plot size, distance to other buildings and

Abbreviations: ATES, Aquifer Thermal Energy Storage; BCI, Building Climate Installation; COP, Coefficient of Performance; GHG, Greenhouse gas.

* Corresponding author.
E-mail addresses: j.m.bloemendal@tudelft.nl, martin.bloemendal@kwrwater.nl (M. Bloemendal).

https://doi.org/10.1016/j.apenergy.2022.118587
Received 14 July 2021; Received in revised form 4 December 2021; Accepted 21 January 2022
Available online 4 February 2022

heating/cooling demand determine the specific effect per building. The optimal well placement policy result from the aquifer utilisation levels discussed above. Maximum GHG emission reduction while maintaining individual ATES system performance, is achieved with well distances of 0.5–1 times the yearly average thermal radius for wells of the same type (cold-cold and warm-warm). Opposite well types (cold-warm) should be placed apart ~2 times the thermal radius to prevent negative subsurface interaction.

Nomenclature

A_A	Surface area of ATES area under consideration [m^2]
B	Energy balance [-]
c_{aq}	Volumetric heat capacity of saturated porous medium; 2.8 × 10^6 [$J/m^3/K$]
c_w	Volumetric heat capacity of water; 4.2 × 10^6 [$J/m^3/K$]
COP	Coefficient Of Performance: ratio between provided thermal energy and consumed electricity [-]
D	Multiplier for thermal radius, to obtain distance (x) between wells [-]
Δp	Hydraulic resistance or required pressure increase [$kg/m/s^2$]
ε	Specific heating/cooling demand [$J/m^2/y$]
E	Energy [J]
f	correction factor [-]
F_s	Allocated aquifer space fraction for ATES [m^3/m^3]
g	Gravitational acceleration; 9.81 [m/s^2]
GHG	Greenhouse gas emissions [kg CO_2]
h	counter for number of buildings with conventional system [-]
i	counter for number of buildings with ATES system [-]
j	counter for number of well [-]
k	number of ATES systems [-]
l	number of conventional systems [-]
L	Well screen length [m]
L_{aq}	Aquifer thickness [m]
m	number of wells [-]
n	Porosity [-]
η_{th}	Recovery efficiency [-]
η_p	Pump efficiency; 0.25 [-]
P	Thermal or electrical power [J/s]
ρ	Water density; 1,000 [kg/m^3]
Q	Hourly pumping rate of ATES wells [m^3/hr]
r	adoption ratio [-]
R_{th}	Thermal radius [m]
t	time [s – hr – d]
T	Temperature [°C]
V_{tot}	Yearly storage volume of groundwater [m^3/y]
x	Distance between wells [m]

Sub-scripts

aq	Aquifer
b	Associated to building
boiler	Associated to boiler energy use/supply
c	Associated to cooling and/or cold well
cap	capacity
cp	Associated to pumps circulating medium inside the building climate installation
cond	Associated to heat pump condenser
dc	Associated to dry-cooler energy use/supply
demand	Associated to energy demand
dense	Dense well placement setting
e	electricity
em	emission
est	estimated
evap	Associated to heat pump evaporator
g	gas
h	Associated to heating
hp	Associated to heatpump
inf	Associated to infiltration in warm/cold well
loss	Associated to heat/temperature losses
max	maximum
min	minimum
o	opposite type of wells
passive	Demand associated with the passive cooling mode
pl	Associated to partial load
r	reference
req	required
s	same type of wells
spacious	Spacious well placement setting
storage	Associated to heating/cooling diverted to the ATES
t	time
tot	total
th	thermal
w	Associated to warm well
well	Associated to the well flow or temperature
y	year

1. Introduction

Heating and cooling of buildings contributes to about 25% of the total worldwide energy end-use [1], hence constituting an important source of greenhouse gas (GHG) emissions. Typical for moderate climates, the demand for space heating and cooling alternates seasonally. Using aquifer thermal energy storage (ATES, Fig. 1) systems for harvesting and storing cooling potential during winter and heating potential during summer, results in fewer emissions for heating and cooling. Low-temperature (LT) ATES systems are therefore increasingly used to reduce primary energy consumption and associated GHG emissions [2]. Worldwide potential for ATES systems exists across Europe, Asia and North-America [2–3]. Life cycle assessment studies indicate that emissions associated to installation activities and component have a negligible contribution to the overall GHG emission of ATES systems [4–5]. Therefore, focussing on operational performance is key in assessing ATES systems.

ATES systems use tube wells[1] to inject and extract groundwater from aquifers in the subsurface. Each system consists of at least two tube wells coupled to a heat exchanger to provide heating/cooling to the building. Around each ATES well the system takes up space in the subsurface where the heat/cold is stored. Interaction between wells of the same type leads to positive thermal performance, while interaction between opposite well types negatively affects thermal recovery efficiency of these systems e.g. Bloemendal et al. [6,38] and Fig. 2. The increasing

[1] please note that environmental hazards related to drilling of ATES wells may differ depending on local geology, and should always be properly addressed

implementation of ATES systems in urban areas has resulted in the (potential) interaction between multiple systems, leading to questions on the impact of their individual performance, optimal use of the subsurface and overall GHG emissions [7–8]. When the wells of neighbouring ATES systems are forced apart to prevent any thermal interaction, this may result in a sub-optimal use of subsurface space for ATES systems and hence lower overall GHG emission reductions [6,9–11]. Under the current legislation in the Netherlands and many other countries, it is not allowed to affect existing ATES systems [12], and 3 times the radius of thermal influence around an ATES well is often used as a distance between wells [7]. The current placement policy prevents a spatially dense positioning of ATES wells. Although Bloemendal et al. [6] and Sommer et al. [13] showed that a higher spatial adoption rate of buildings with ATES, leads to an overall reduction of GHG emissions, and smaller distances are also applied in practice, it is still unclear how severe the poorer performance of ATES systems is due to interaction between ATES wells and how this leads to higher primary energy use for buildings that are affected by new neighbouring ATES systems. Furthermore, it is not yet clear how changes in individual ATES system GHG emission relate to the overall decrease in GHG emissions for the entire region.

Therefore, the goal of this study is to assess how the different well placement scenarios lead to subsurface interaction between ATES wells and how these interactions affect the individual primary energy use and GHG emissions of each specific building as well as overall GHG emissions. The insights from this study aim to foster practical planning and design rules suitable to ensure optimal ATES utilisation with improved GHG emissions reduction while preventing negative impact on the primary energy use of individual buildings with ATES, which is crucial for the societal and governmental support of high density placement policies.

1.1. General approach

A simulation study is carried out to evaluate the primary energy use of buildings with ATES systems under spacious and dense ATES well placement policies. To identify optimal well placement rules while evaluating individual performance of ATES systems, 3 aspects are important to take into account:

1. The building characteristics (thermal requirements, building plot space), because they determine the number of wells needed and the available plot space for well placement.
2. The performance of the ATES wells and their interaction between neighbouring wells.
3. The primary energy use of the building facilities following from the ATES well performance.

The calculated GHG emissions for individual ATES users and the total emissions for all buildings in a case study area are evaluated using an analysis of the energy use of the building climate installation for which a detailed building climate installation (BCI) model is developed and validated. This BCI model simulates the energy flows of the buildings during the simulation period and tracks the primary energy use of the buildings in the study area. The subsurface interactions between the ATES wells in the model are simulated with an existing groundwater model code [6,38], which is fully integrated with the developed BCI model. Placement of ATES wells is done with an agent based model, to assess various placement policies while taking into account spatially constrains in the well placement procedure such as e.g. buildings, infrastructure and surface water [14]. For the spatial distribution and thermal requirements of 26 unique buildings as present in the city centre of Utrecht, the ATES system density is varied using an agent-based approach applying various placement restrictions, within which ATES adoption order and well placement was randomized. Well placement density is varied for 9 scenarios by changing the distance between wells of the same and the opposite type taking into account the thermal storage volumes that would be required for the adoption of ATES by an individual building.

2. Methods

2.1. Well placement based on thermal radius

During infiltration in an ATES well, a cylindrical shaped volume of warm/cold groundwater is formed around the well (Fig. 3). This is called the thermal radius (R_{th}) and is calculated based on the total seasonal storage volume of a well:

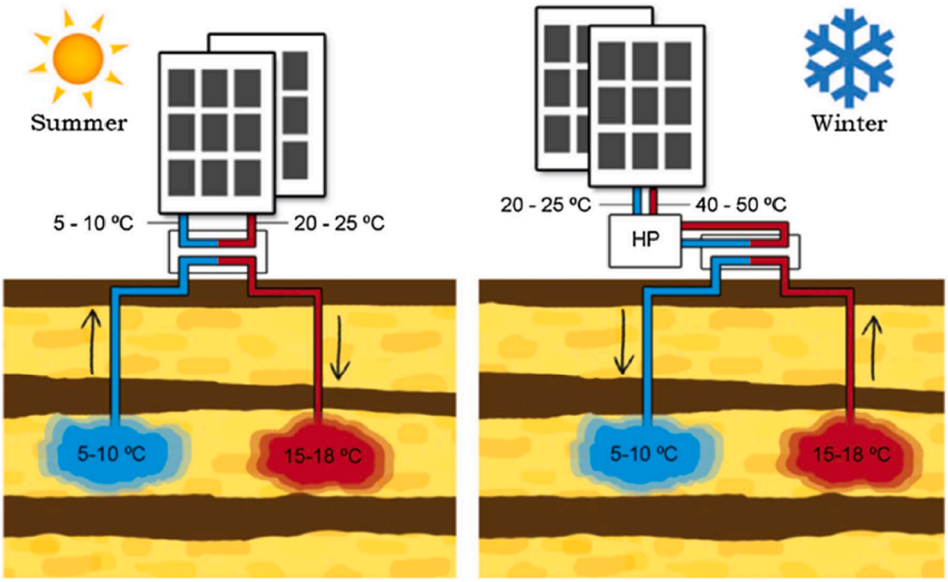

Fig. 1. Basic working principle of a low-temperature (LT) ATES-doublet. Right: In winter, buildings are heated with a heat pump (HP) which extracts heat that was previously stored in the warm well. This creates cooling capacity which is stored in another well in the subsurface. This cooling capacity is used in summer (left) to cool the building, by storing the excess heat in the warm well. From: Bloemendal et al. [6].

$$R_{th} = \sqrt{\frac{c_w V}{c_{aq} \pi L}} \quad (1)$$

With c_w and c_{aq} being the volumetric heat capacity (J/K/m^3) of water and the saturated aquifer, V the total injected volume (m^3) and L the aquifer thickness (m). In a given area, the aquifer thickness and volumetric heat capacity are often assumed to be constant. The building heating/cooling demand and associated infiltration/abstraction volume therefore determines the variation in size of the thermal radius and the number of used wells. Distance between wells of the opposite type (x_o) and same well types (x_s) is calculated as a function of the thermal radii of the two wells [6]:

$$\begin{aligned} x_o &= D_o \cdot \overline{R_{th}} \\ x_s &= D_s \cdot \overline{R_{th}} \end{aligned} \quad (2)$$

Well placement policies follow distance rules which depend on these thermal radii: wells of the same type (D_s) can be placed closer to each other, while wells of the opposite type (D_o) should be placed further apart, Fig. 3. When wells do not have the same thermal radii, the distance between wells is calculated based on the average of the two thermal radii. A combination of values for D_o and D_s is defined as a placement policy or scenario. For convenience and simplification reasons the abbreviations $x_s = 2{*}R_{th} \rightarrow$ '$D_s = 2$' and similarly $x_o = 3{*}R_{th} \rightarrow$ '$D_o = 3$' are used in this study. This approach allows for representative translation of the results of this study to other locations with a wide range in aquifer thickness available for ATES.

2.2. Modelling approach

The coupled simulation framework is programmed in python code, which is a commonly used scripting language in science and engineering [15]. This framework uses two external simulation codes: MODFLOW/MT3DMS for groundwater temperature simulations section, section 2.2.3, [16–17] and agent based model NetLogo for the well placement, section 2.2.2 [18]. Additionally, a Building Climate Installation (BCI)

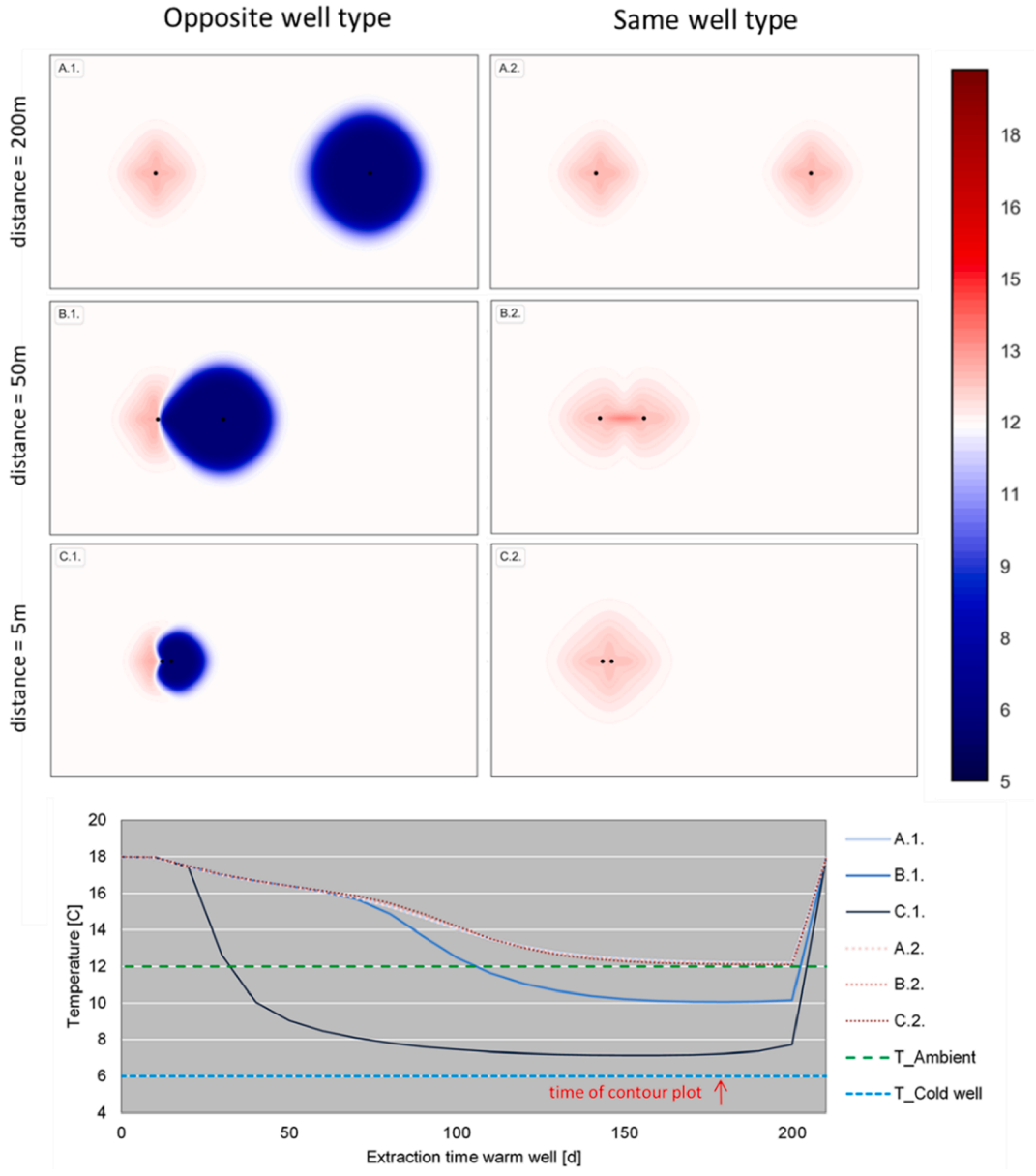

Fig. 2. Schematic top view of how two wells of the same and the opposite type interact at various distances from each other. Distances between wells: top: 200 m, middle: 50 m. lower: 5 m. The bottom graph shows the left well (warm well in both cases) temperature development during extraction for the 6 cases, the presented well temperature plots are at the end of extraction from the warm well.

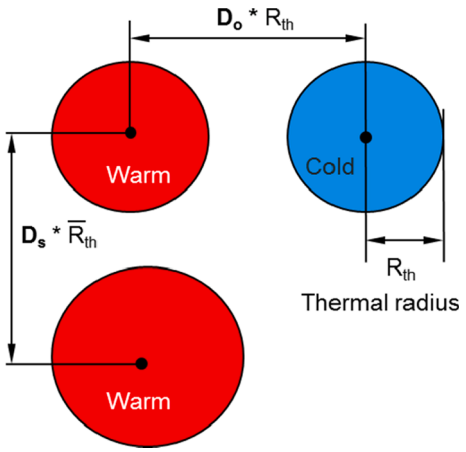

Fig. 3. Schematic overview of distance rules between wells of the same (D_s) and the opposite (D_o) type based on the thermal radius (R_{th}) [32].

model is developed to A) calculate energy demands for each building in the simulation and to B) subsequently determine primary energy use of each component of the BCI (section 2.2.1). During simulation, the BCI is coupled to the groundwater model. The simulation procedure is schematically depicted in Fig. 4 and consists of two main steps:

1. Initialisation: Like is done in practice, a reference climate year is used to calculate the energy demand and sizes of the ATES system and BCI components for each building. The NetLogo model is used to initialize the well locations depending on the predefined well placement policy. If there is no space to place a minimum of 2 wells for the ATES system, a conventional BCI is assigned to those buildings for that specific simulation.

2. Simulation: The building-climate model and MOFLOW model are run subsequently for each hourly time-step of the simulation period. The building-climate model serves as an input for the MODFLOW model and vice versa.

2.2.1. Building climate installation

The main functionality of the BCI model is to correctly represent the interaction between the ATES system and the building climate installation, as well as conventional climate installation for heating and cooling. Therefore, two BCI models are created, one for buildings with an ATES system and one for conventional buildings, Fig. 4. Conventional heating and cooling systems consists of a gas boiler for heating and a chiller, which uses electrical energy, for cooling. The ATES system BCI model is described in the remainder of this section. For simplification reasons, the ATES system BCI is described for one building with one doublet (1 warm and 1 cold well), please note that the model infrastructure can handle any type and number of buildings with any number of ATES well doublets.

The ATES system BCI model is a conceptual model with components and operation modes according to Dutch design standards for ATES systems, Fig. 5 [19–20]. The main components of the ATES system BCI are the heat pump, which directly interacts with the ATES wells, the dry cooler to exchange heat or cooling capacity with the outside air and a peak boiler, Fig. 5. Each building has these same components and modes of operation, due to differences in size and function of the building the energy demand varies and with that also the size of components.

2.2.2. Basic description of ATES climate installation

An ATES system consists of a cold and a warm well connected to a heat pump (HP) via a chilled water net and a heat exchanger. Tube wells produce and inject groundwater. Submersible pumps use electricity to pump the groundwater from one well to another via a heat exchanger which allows for heat exchange with the BCI. In summer (cooling demand), cold groundwater is used directly for cooling, Fig. 5-A. In winter (heating demand) the heat pump condenser provides heating at the required temperature level, while at the evaporator side of the heat pump heat is taken from the warm well, cooling down the groundwater, hence cooling capacity is stored in the cold well, Fig. 5-B. To operate, the heat pump uses electricity. In summer, the heat pump is mostly not used, because free cooling is used directly from the cold well. But, when the cooling capacity of the cold well is not sufficient, the HP can be used to

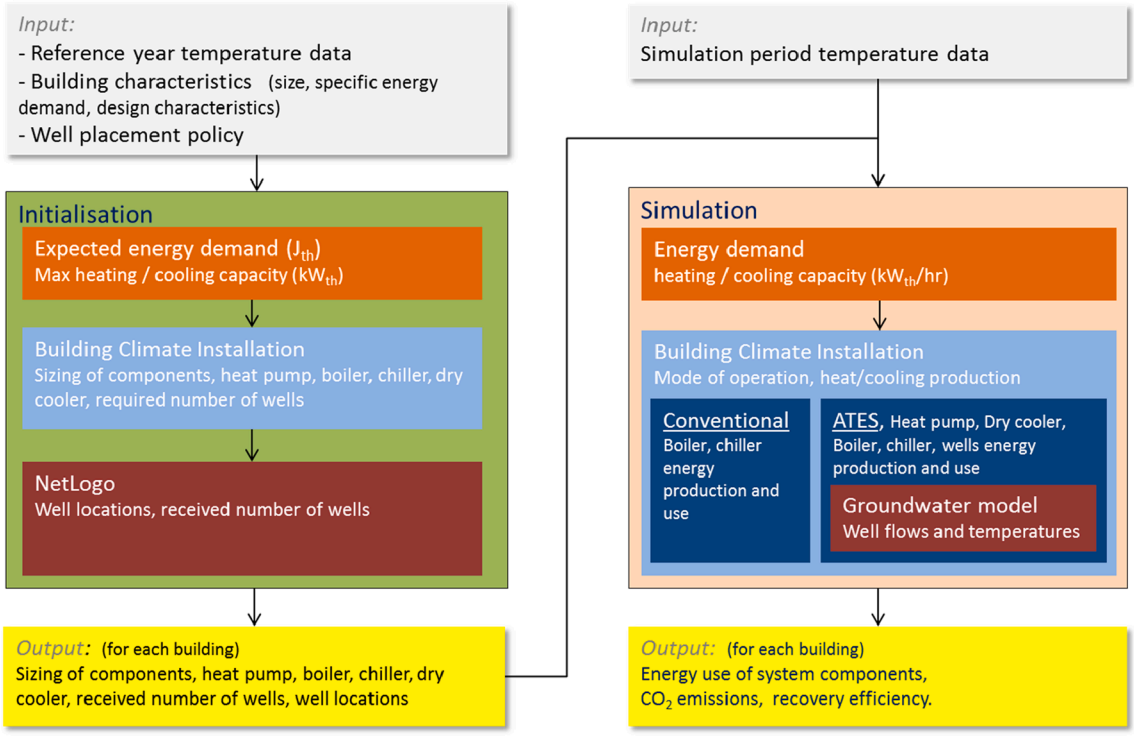

Fig. 4. Schematic representation of the simulation framework of the different components of the used modelling system.

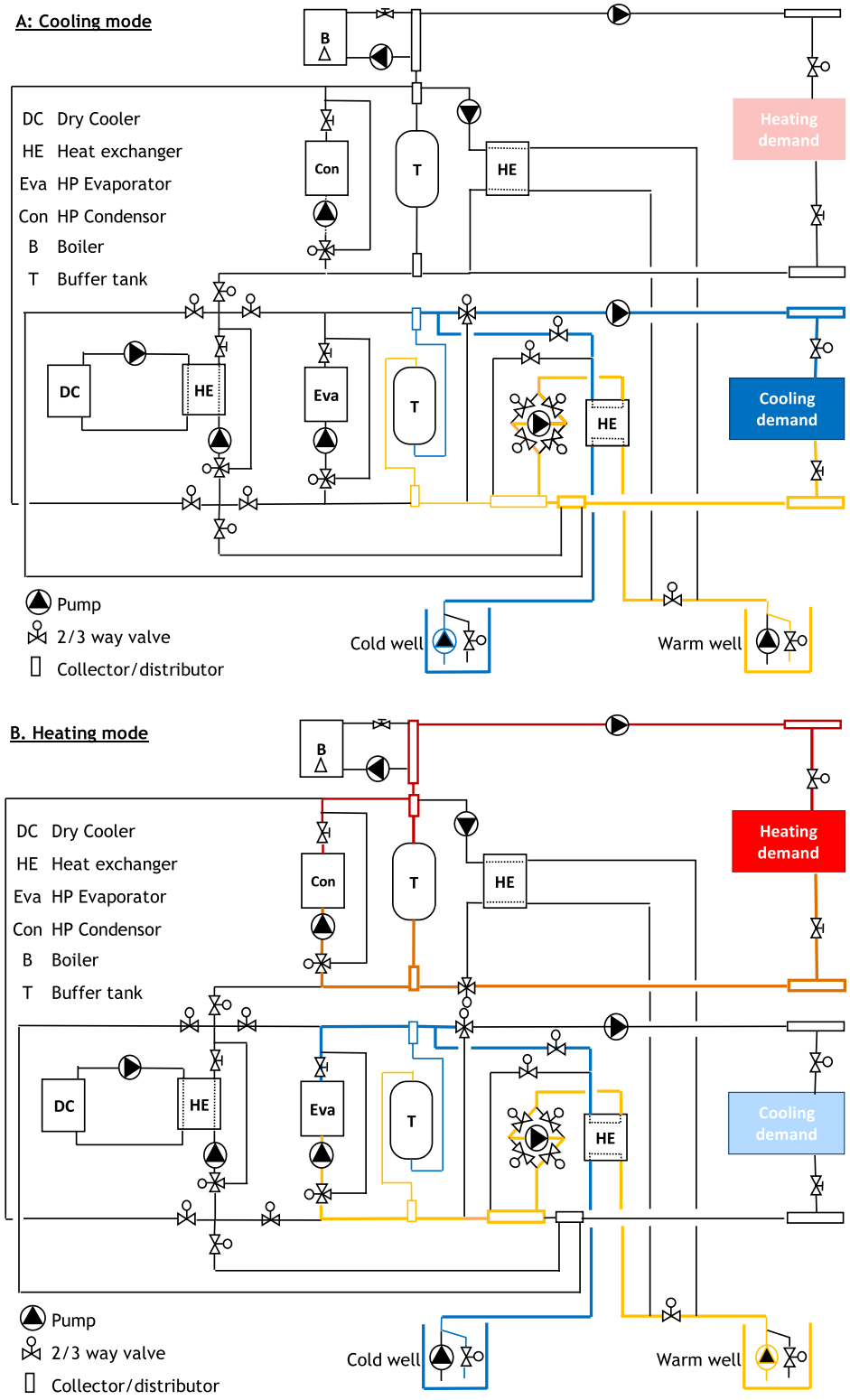

Fig. 5. Climate installation schematics, depending on heating/cooling demand conditions different modes of operations may exists. The condenser (Con) and evaporator (Eva) together represent the heat pump. Two out of five possible modes are illustrated. A: cooling mode: cooling is directly delivered from the cold well, the buffer tank is used to prevent frequent switching of the submersible well pump. When cooling capacity from the cold well is insufficient, evaporator of the heat pump delivers cooling, depending on the ATES energy balance condition the heat produced at the condensor is either dispersed into atmosphere via the dry cooler, or stored in warm well. B: heating mode: warm groundwater is used by the heat pump evaporator, condenser provides heat to the distributor demanding heat. When warm well/ heat pump cannot deliver the required heat capacity, the peak boiler add extra heat.

provide extra cooling capacity to the building. Cooling capacity from the evaporator is provided to the building, the heat produced at the condenser side is then stored in the warm well or dumped to the outside air via the dry cooler. In case of simultaneous heating and cooling demand (not shown in Fig. 5), heat produced at the condenser and cooling capacity from the evaporator are both supplied to the building. The ratio between heating and cooling demand will determine whether the ATES supplies additional heat to the heat pump or direct cooling to the building. When heating and cooling demand of the building is not in balance over multiple years a dry cooler[2] is used to either store extra heat in summer or extra cooling capacity in winter, to meet the next

[2] Instead of a dry cooler also other techniques can be used, asphalt or solar collectors, or surface water. Their energy use varies little and depends on local conditions. Therefore only the dry cooler is evaluated in this study.

seasons' energy demand. Dry cooler operation requires electricity use of circulation pumps and ATES well pump. The heat pump is installed at around 35–50% of maximum required heating capacity and then provides ~80% of the total heating demand (Fig. 6). The remaining ~20% is provided with a boiler which uses natural gas. This is done in practice to save costs because a monovalent ATES systems requires a significantly larger heat pump and double the ATES wells capacity, which is more expensive.

2.2.3. Temporal discretization and simulation horizon

The model simulates the BCI parameters at an hourly time steps, which is the minimum needed time step to account for diurnal variations in energy demand. This therefore also requires hourly temperature data input.

The total simulation horizon is set to 5 years. Although this is shorter than the expected life span of ATES systems, it is sufficiently long to distinguish between performance under varying well placement policies [21–22].

2.2.4. Initialisation: Energy demand of buildings

The energy demand of each building is identified using the gross surface area of the building and the estimated specific yearly heating and cooling demand from a Dutch database (RVO). The total demand is then subdivided to hourly rates using both the outside air temperature of a reference year and the characteristics of the specific building (e.g. opening hours). The detailed calculation sub-steps are presented in appendix I. The result of this step is that each building in the simulation has an expected hourly heating and cooling demand which varies among each building because building functions, opening hours and size vary. Based on the maximum hourly values for heating and cooling demand the required size of the heat pump is determined.

2.2.5. Initialisation: Sizing of components

2.2.5.1. Heat pump. Depending on the type of ATES system BCI: monovalent or bivalent, the size of the heat pump is determined. In case of a bivalent system, the HP is designed to provide 35% of the maximum required heating capacity, Fig. 6. In such conditions the HP can still provide the vast majority of the heat, because the maximum capacity is only needed during a limited amount of time during the year, Fig. 6. When choosing a monovalent system, the heat pump needs to cover 100% of the required capacity. Thus, the HP properties follow from the maximum required heating capacity found for each building in the reference year calculation and the setting for the required heat pump capacity and Coefficient of Performance (COP), Table 1.

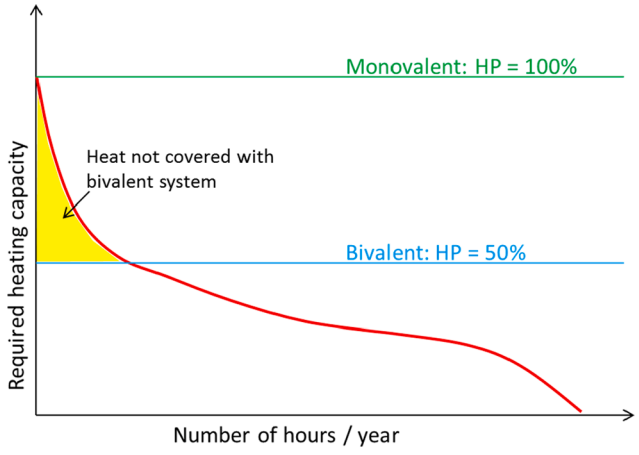

Fig. 6. Heat pump design: monovalent versus bivalent.
Adapted from: [36]

Table 1
Parameters settings used for the BCI model.

BCI parameter	Value	Description
$T_{c\_return\_min}$ [°C]	13	The minimum return temperature from the building after passive cooling (cold well > warm well).
$T_{c\_return\_max}$ [°C]	16	The maximum return temperature from the building after passive cooling (cold well > warm well).
T_{w_supply} [°C]	45	Supply temperature to the building for heating
T_{w_return} [°C]	35	Return temperature from the building after heating
Q_{well_max} [m^3/h]	100	Maximum well pumping capacity
$T_{inf\_w\_max}$ [°C]	25	Maximum infiltration temperature during cooling (cold well > warm well)
C_1 [-]	0.001604	Heat pump correction parameters, used to calculated
C_2 [-]	0.739065	the heat pump correction factor that is used to
C_3 [-]	9.624631	calculate the electricity use of the heat pump under varying partial loads.
T_{evap_c} [°C]	8	Evaporator exit temperature during heating
F_{pl_min} [-]	0.25	The minimum partial load of the heat pump
T_{loss} [°C]	1	The temperature loss in the heat exchanger.
COP_{dc} [-]	25	The COP of the dry cooler
COP_C [-]	3	The COP of the chiller that is used by the BCI to cool building without an ATES system.
COP_{HP} [-]	5	The COP of the HP at full load
$COP_{circulation}$ [-]	75	The COP for circulation pumps
COP_{well} [-]	40	The COP of the well pump during heating/cooling
COP_{boiler} [-]	0.825	Energy efficiency of the gas boiler, based on upper calorific value Dutch gas mix[1]

[1] For clarity/uniformity reasons in this study COP is used as a symbol instead of the usual η or EER for boilers

2.2.5.2. Number of wells. The required number of wells (m_{needed}) for each building follow from the maximum flow needed to provide the required cooling capacity and heating capacity (P_{h/c_i_max}) from the wells, please note that the maximum capacity from the warm well depends on size and COP of the heat pump. The temperature difference between the wells (ΔT) and the volumetric heat capacity of water (c_w) determines the required flow capacity from the wells (Q_{req}). It is assumed that the aquifer of choice in the study area can host wells with a capacity of $Q_{max} = 100\ m^3$/hr, the number of wells follows from dividing the required capacity by the maximum flow rate per well. If the required number of wells (m_{needed}) is actually available depends on the NetLogo well placement following the determined well placement policy.

$$m_{needed} = \frac{Q_{req}}{Q_{max}} = \frac{P_{h/c\_i\_max}}{\Delta T \cdot c_w \cdot Q_{max}} \quad (3)$$

N.B. In any case no maximum is set to the chiller (when no ATES wells can be placed) boiler and dry cooler size. For the interaction and energy use of these components it doesn't matter what capacity/size they have.

2.2.6. Simulation: BCI operation dynamics

The climate installation model consists of a series of calculations to determine the functioning and energy use of the different components of the installation. The building energy fluxes described below are calculated and saved for each hourly time step (t) for each individual building (k). Each variable is not explained individually in the text, the nomenclature gives the description of the used variables, constants and subscripts. The scheme in Fig. 7 is the blueprint for the calculations explained in the 10 steps described below.

1. Maximum passive cooling

To determine the amount of passive cooling that can be provided by the system under a given cooling demand, the maximum passive cooling needs to be calculated. To calculate this, the expected infiltration temperature in the warm well due to passive cooling ($T_{inf\_w\_est}$) is estimated:

$$T_{inf\_w\_est} = T_{c\_return} - T_{hex\_loss} \quad (4)$$

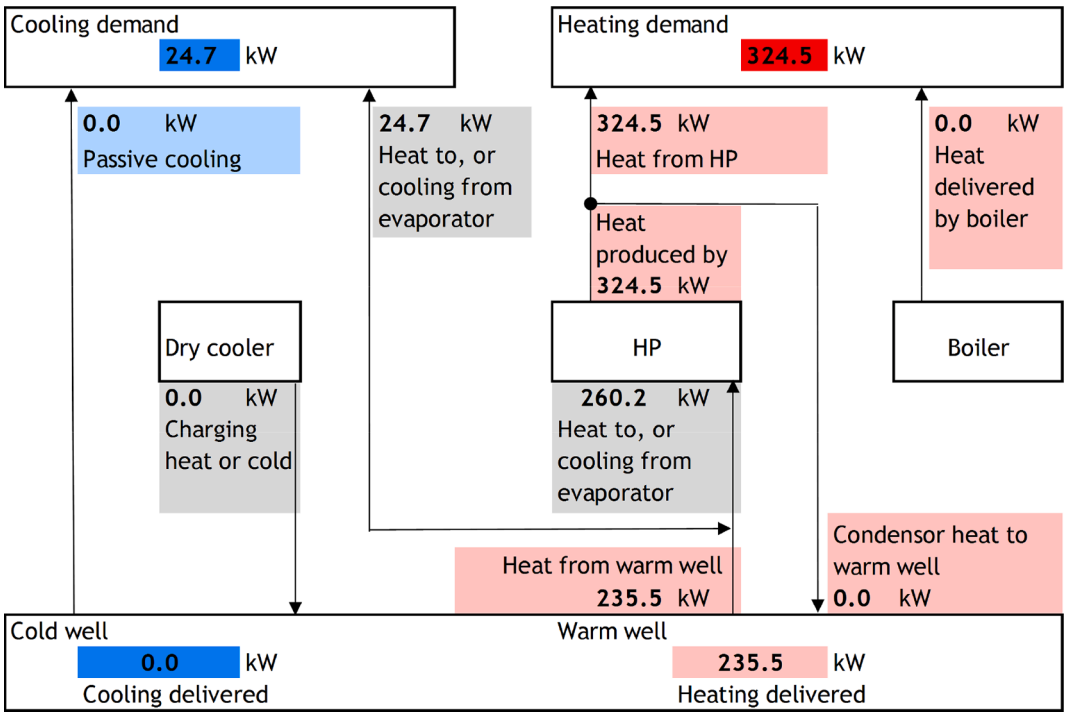

Fig. 7. Schematic of BCI component functioning during one hour in winter (heating demand).

Where T_{c_return} is the return temperature of the cooling grid inside the building and T_{hex_loss} is the temperature loss over the heat exchanger. T_{c_return} varies between a minimum temperature ($T_{c\_return\_min}$) at low cooling capacities and a maximum return temperature ($T_{c\_return\_max}$) at maximum cooling capacities. T_{c_return} is determined by the size of the cooling demand divided by the maximum cooling demand:):

$$T_{c\_return} = T_{c\_return\_min} + \frac{E_{c\_hr} \cdot (T_{c\_return\_max} - T_{c\_return\_min})}{E_{c\_h\_max}} \quad (5)$$

The maximum amount of passive cooling ($P_{ATES\_c\_passive\_max}$) is subsequently calculated as:

$$P_{ATES\_c\_passive\_max} = Q_{ATES\_w\_max} \cdot m \cdot \frac{c_w}{\Delta t} \cdot (T_{inf\_w\_est} - T_{well\_c}) \quad (6)$$

With c_w being the heat capacity of water, m the number of wells for the building under consideration and time step size (Δt), in this simulation one hour.

2. Maximum total heating & maximum condenser power

The maximal ATES total heating capacity ($P_{ATES\_w\_max}$) is calculated based on the temperature difference between the warm well and the infiltration temperature in the cold well, the latter being a fixed set point of the heat pump.

$$P_{ATES\_w\_max} = Q_{ATES\_w\_max} \cdot m \cdot \frac{c_w}{\Delta t} \cdot (T_{well\_w} - T_{inf\_c}) \quad (7)$$

During high cooling demand, passive cooling capacity can be insufficient, in this case the heat pump can be used to provide extra cooling demand. This results in an amount of condenser heat. The maximum amount of condenser heat that can be stored in the wells is given by:

$$P_{ATES\_cond\_max} = (Q_{ATES\_c\_max} \cdot m \cdot \frac{c_w}{\Delta t} \cdot (T_{inf\_w\_max} - T_{well\_c})) - P_{ATES\_passive\_max} \quad (8)$$

3. Calculation of partial load of the heat pump

The heat pump usage is a percentage of the maximum heat pump capacity and can therefore never be higher than 100%. The heat pump can be used for both cooling and heating. The partial load factor (f_{hp_pl}) of the heat pump is determined by the heating/cooling demand, size of the heat pump and the temperature of the warm and the cold wells. Considering that all heat demand is supplied by the heat pump and all excess heat of the condenser is stored in the ATES system at peak cooling, the partial load of the heat pump is determined by the minimum and maximum partial load conditions of both the evaporator and condenser. The maximum partial load factor of the condenser capacity is calculated by: $f_{pl\_cond\_max} = \frac{(P_h + P_{ATES\_cond\_max})}{P_{cond\_max}}$ (9)

In which P_h follows from the hourly heating demand E_{h_t}, divided by one hour. The maximum partial load of the heat pump evaporator is calculated using the cooling demand and the maximum thermal capacity of the warm well (both are connected to the heat pump evaporator):

$$f_{pl\_evap\_max} = \frac{(P_c + P_{ATES\_w\_max})}{P_{evap\_max}} \quad (10)$$

The minimal partial load of the heat pump evaporator is calculated by:

$$f_{pl\_evap\_min} = \frac{(P_c - P_{ATES\_passive\_max})}{P_{evap\_max}} \quad (11)$$

The partial load of the heat pump condenser based on the actual heat demand is calculated by:

$$f_{pl\_cond\_demand} = \frac{P_h}{P_{cond\_max}} \quad (12)$$

In practice, there will also be a minimal partial load at which the heat pump can still operate. In this model, it is assumed that in such a case, excess heat or cooling capacity is stored temporarily in a buffer tank in the plant room. This buffer is not modelled, but partial loads between 0% and 100% are allowed instead.

4. Condenser / Evaporator power of the heat pump

Based on the calculated partial load of the heat pump, the actual

condenser and evaporator power can be calculated as:

$$P_{cond} = f_{hp\_pl} \cdot P_{cond\_max} \text{ and } P_{evap} = f_{hp\_pl} \cdot P_{evap\_max} \quad (13)$$

5. Heat pump operation

From the calculated heat pump operation it is now calculated how much will be stored in the wells. When the heating demand is smaller than the condenser heating capacity, the amount of stored heat is calculated as the condenser heating capacity minus the heating demand. Similarly, the amount of stored evaporator capacity is the difference between the cooling demand and the available evaporator capacity.

During heating, the amount of heat that needs to be supplied by the boiler is:

$$P_{boiler} = P_h - (P_{cond} - P_{cond\_storage}) \quad (14)$$

During cooling, the amount of passive cooling that is delivered is determined by the heat pump is calculated as:

$$P_{c\_passive} = MIN(\mathrm{P_{ATES\_passive\_max}}, (\mathrm{P_c} - (\mathrm{P_{evap}} - \mathrm{P}_{evap\_storage}) \quad (15)$$

6. Energy flows Heat Pump

Similarly the required heating/cooling capacity from the ATES wells follow from the heat pump operation. The evaporator power therefore defines the needed capacity from the warm wells ($\mathrm{P_{ATES\_h}} = \mathrm{P_{evap}}$) and the needed capacity from the cold wells is defined by the sum of passive cooling capacity and the stored warm energy at the condenser. The residual heating/cooling directly utilized from the heat pump is calculated as the evaporator capacity minus the heating capacity.

7. Volume flow from ATES wells (injection & extraction)

The amount of volume that is extracted from a type of well and is injected into the other type of well depends on the total energy flow and the ΔT between injection and extraction. In heating mode, the injection temperature is known (set at certain temperature, e.g. 6 °C). During cooling, the injection temperature is not exactly known but is estimated in step 1. The volume flow is subsequently calculated as for cooling:

$$Q_c = \frac{\Delta t \cdot P_{c\_passive}}{(T_{c\_return} - T_{well\_c} - T_{loss}) \cdot c_w} \quad (16)$$

And for heating as:

$$Q_h = \frac{\Delta t \cdot P_{ATES\_h}}{(T_{well\_w} - T_{inf\_c}) \cdot c_w} \quad (17)$$

8. Infiltration temperature of warm and cold well

An important parameter for the interaction with the groundwater model is the temperature of the infiltrated thermal energy. For storage at the cold well a fixed temperature is set, which is similar like in practice; the temperature of the evaporator of the heat pump, plus a temperature loss that occurs in the heat exchanger

$$T_{inf\_c} = T_{evap\_c} + T_{loss} \quad (18)$$

With (T_{loss} is 1 °C in this study). Heat injection is not as straightforward. During cooling different modes of operation may occur, which together result in an injection temperature for the warm well. Low capacity passive cooling yields relatively low injection temperatures (e.g. 14 °C) while high capacity passive cooling results in relatively high temperatures (e.g. 17 °C). In case of peak cooling demands, condenser heat of the heat pump (functioning as chiller) will increase the injection temperature even further:

$$T_{inf\_w} = T_{well\_c} + \frac{\Delta t \cdot P_{ATES\_c}}{Q_c \cdot c_w} \quad (19)$$

9. Energy balance of the wells

When the wells of the ATES system are not in balance the climate installation model will respond to this and will force the ATES system to restore the energy balance. This is done with the dry cooler and can only be done if the outside air conditions are suitable, in winter it is only possible to store extra cooling capacity and in summer heating capacity. First the required heating and cooling capacity is delivered, the remaining capacity of the wells can be used for energy balance corrections. The energy balance (B) is assessed after a period of continuous operation of 2 years. When the imbalance is >15%, the ATES system will use its dry cooler capacity to store more heat or cooling capacity.

$$B = \frac{E_h - E_c}{E_h + E_c} \quad (20)$$

$B < 0$: cold well is growing, more heat needs to be charged to the ATES wells.

$B > 0$: warm well is growing, more cold water needs to be charged into the wells.

Restoring the energy balance can be done when $Q_{h/c} < Q_{max}$. When this is the case, the available amount of pumping ($Q_{max} - Q_{h/c}$) will be used to store extra heat or cooling capacity. This is done with the temperature calculated in the previous step (T_{inf_w} / T_{inf_c}).

$$P_{dc} = \frac{(Q_{max} - Q_h) \cdot c_w \cdot \Delta T}{\Delta t} \quad (21)$$

10. Determine Energy use HP, Dry cooler, boiler, circulation pumps

From the operation modes identified in the previous calculation step the energy use of each component for each hourly time step can now be calculated. For the dry cooler (E_{dc}), circulation/well pumps (E_{wp}, E_{cp}) and boiler (E_{boiler}) this is straightforward:

$$E_{boiler\_hr} = \frac{P_{boiler}}{COP_{boiler}} \cdot \Delta t \quad (22)$$

$$E_{dc\_hr} = \frac{P_{dc}}{COP_{dc}} \cdot \Delta t \quad (23)$$

$$E_{wp\_hr} = \frac{P_{ATES\_c} + P_{ATES\_h}}{COP_{well}} \cdot \Delta t \quad (24)$$

$$E_{cp\_hr} = \frac{P_{ATES\_c} + P_{ATES\_h}}{COP_{circulation}} \cdot \Delta t \quad (25)$$

In the calculation of energy use by the circulation pumps are included the pumps for circulation in evaporator, condenser, boiler, dry cooler, heat exchangers and circulation circuit to the building for both heating and cooling mode.

The energy use of the heat pump depends on the quality of the source and is not linear, at partial load the electricity use is lower than at full capacity and the COP is therefore higher at that moment. To take this into account the heat pump COP is corrected with a factor y_{hp} (Fig. 8). The electricity consumption of the heat pump is calculated using the following equation:

$$E_{hp\_hr} = f_{hp} \cdot \frac{P_{hp\_max}}{COP_{hp}} \cdot \Delta t \quad (26)$$

The electricity use of the heat pump is corrected with the factor f_{hp}. This is calculated following the relationship shown in Fig. 8. This relationship is determined from heat pump data (Appendix II).

Please note:

- In this study, we use a constant COP for the well pump and the circulation pump. In practice, the well and circulation pumps may have

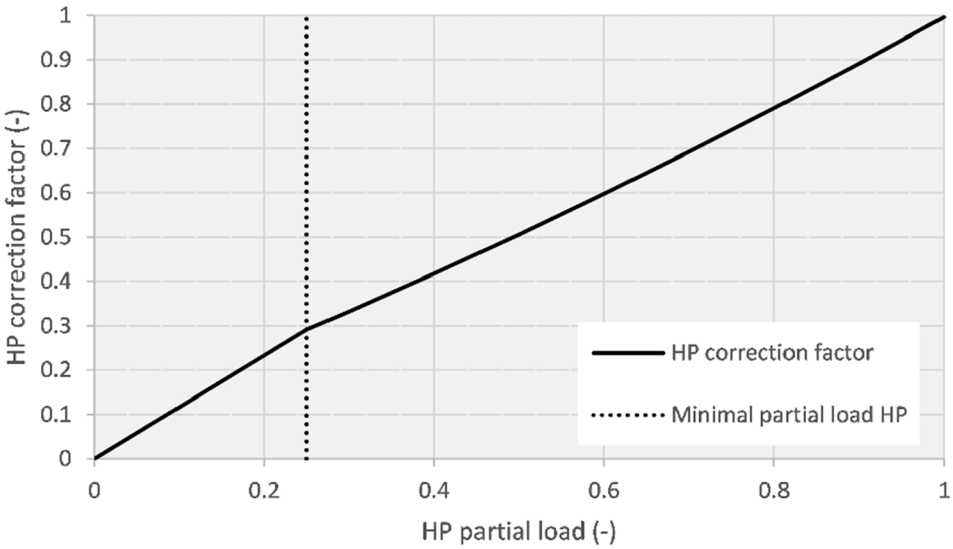

Fig. 8. The heat pump correction factor for the range of possible partial loads of the heat pump, used to calculate the electricity use of the heat pump.

a limited variation in COP. Our results show that the energy use of these components is relatively small. Hence applying a constant COP for well and circulation pumps has limited impact on the results.

- Chiller COP, could be considerably lower under partial load conditions, and thus affect results. Because the chiller is mainly used in the conventional BCI, running it with a constant best case COP will underestimate the electricity use of the chiller. Therefore, this is a worst-case situation for comparing ATES to conventional. Adding chiller COP variability would not seriously change the results and conclusions of this study, it would make the results more in favour of high density ATES.
- Boilers under partial load will have a lower efficiency than boilers running in full load. In this study, boilers run in partial load. For gas boiler, lower but constant value for efficiency are used due to partial load.

2.2.7. *Placement of wells with NetLogo*

Agent based modelling is used to model the systematic outcomes that emerge from the behaviour of individual actors (in this case building owners) and is used for socio-environmental simulation of common pool resource problems like groundwater for ATES utilisation in cities [8,14].

For this study NetLogo is used to initialize ATES wells with their placement behaviour during initialisation in a pre-defined area. Each agent is characterized by the size and function of the buildings in the study area. The number of wells and the size of each ATES system follow from the energy demand and size of components of the BCI. The following placement procedure is implemented in NetLogo to represent the stochastic nature of ATES adoption dynamics:

- The study site is divided in 1x1m patches, each patch can be used by buildings to place a well. Each building in the study site has been appointed a plot in the NetLogo environment; the buildings can only build wells on free patches within their plot and adjacent sidewalks.
- The placement of new ATES systems is in random order. New ATES system choose a random location for one of its wells from the available patches in their plot, respecting the placement rules with already existing ATES wells. The other well of this system is then placed in the plot respecting the placement rules. The patches around each well can no longer be used for placement of other wells, depending on the size of the well and the placement rules, Fig. 9. Each ATES system installs its wells using this procedure resulting in success when there was available space, or in failure when the wells couldn't find a location in the grid while respecting the placement rules.
- During placement of new ATES systems, less and less space remains available to place new wells, as a space around each well is required around to prevent mutual interaction. If only a limited space was available for well placement, this can results in a lower amount of placed well doublets than was originally planned (calculated during ATES initialisation).
- Within the imposed spatial constraints, ATES systems continue to be added until no more well locations can be found because the area is filled with ATES wells and separation space between wells.

Fig. 9. Example output of the Agent Based model: placement of 39 well pairs (78 total wells).

Due to the stochastic nature of the simulation in agent based modelling, a single simulation realization is not representative. Therefore, each scenario comprises of 24 complete model realizations; model testing has showed that with 24 realizations per scenario the distribution of the results was sufficiently stable to confirm representative behaviour

suitable for analysis. Using this approach to assess different placement policies for ATES wells allows to translate simulation results also to other areas, because the stochastic uncertainties associated with different city lay-out are taken into account when assessing the ensemble results, rather than individual model realizations.

2.2.8. Geohydrological modelling with MODFLOW/MT3D-MS

The geohydrological model used for simulation of the subsurface interactions between ATES systems is MODFLOW/MT3D-MS run through the SEAWATv4 model. SEAWATv4 combines MODFLOW (groundwater flow simulations by using a finite-difference method [23] and MT3DS (Multi-Species modular 3D transport model [17]). Because of the similarity between the equations for solute and heat transport, MT3DMS can be used to model transport of heat, by treating heat as a solute species [24–25]. The MODFLOW/MT3DS model is used to simulate subsurface flow with heat transport, to obtain the extraction temperatures of the wells to be fed into the BCI model. Subsurface conditions are considered homogenous. The FloPy model, is used to build and run these models in python [26].

2.2.8.1. Spatial discretization. For this study the thermal distribution and heat loss in the horizontal plane is of interest, while vertical loss is not. Vertical distribution and losses to confining layers is also expected to be relatively small compared to horizontal losses [21–22]. Therefore, using only 1 layer in the vertical direction with the height of the total aquifer thickness (26 m) will not affect the interaction effects between the wells of interest in this study while limiting the model complexity and required computational resources [6].

To accurately calculate horizontal movement of groundwater and thermal energy, the city centre of Utrecht was modelled with a 2.5x2.5 m grid in the area of the building locations. A zone of 100 m with the same cell sizes is constructed around the well-area to minimize numerical dispersion. Around this area the model extents for another1000m with a logarithmically increasing cell size up to a maximum of 200 m at the grid boundaries. This results in a model grid with an extent of 3500x3500m (Fig. 10). The resolution at the area of interest stays well within the minimum required cell-size of 5x5m identified by Sommer et al. [22] to adequately model the heat transport around ATES wells. A description of the subsurface and geohydrological conditions is provided in Appendix III.

2.2.8.2. Initial and boundary conditions. Model boundaries are set to have fixed heads and temperatures at the boundaries. Ambient temperatures are set at 12 °C, which is the assumed average ambient groundwater temperature of the shallow subsurface. Initial and starting heads are set to surface level of the model and are constant at model boundaries.

2.2.8.3. Parameter settings. Aquifer properties are homogeneous because the effect of heterogeneity on ATES well recovery efficiency is shown to be insignificant [27–29] and may disturb the analysis of the subsurface interactions. Influence of buoyancy flow due to density difference that occur due to temperature differences are negligible for LT-ATES and is therefore not taken into account [21,30–31]. Because hydraulic conductivity has negligible effects on thermal losses under homogeneous conditions [21], the horizontal and vertical hydraulic conductivity is set to a constant value of 30 m/d and 6 m/d respectively. Both are common values for the aquifers found in the Netherlands (anisotropy factor of 5). The other thermal and numerical parameters follow literature values and are given in Table 2.

2.2.9. Combined model validation

The BCI model results are aggregated over the time step length at which the groundwater model runs, which is 30 days. This results in a net flow and weighted averaged infiltration temperature, which functions as input for the MODFLOW/MT3D-MS model which subsequently simulates the subsurface changes for the next time step. Thereafter, well temperatures are used as input for the climate installation model. It is computationally expensive and time consuming to also run the groundwater model at hourly time steps. This is not needed because the groundwater systems reacts slower to dynamics of the climate installation. Test runs with time steps of the groundwater model of 5 days, a week and a month were carried out, which gave no significant difference in outcomes, indicating that monthly time steps are sufficiently small to assess well performance under varying well placement policies and capture seasonal storage cycle dynamics. Please note that MT3D-MS

Table 2
MODFLOW simulation parameters [24–25,27]

Parameter	value	unit
Porosity	0.3	–
Longitudinal dispersion	1	m
Transversal dispersion	0.1	m
Horizontal conductivity	30	m/d
Vertical conductivity	6	m/d
Bulk density	1889	kg/m^3
Bulk thermal diffusivity	0.16	m^2/day
Specific heat capacity solids	750	J/kg °C
Specific heat capacity water	4183	j/kg °C
Thermal conductivity solid	3	W/m °C
Thermal conductivity water	0.61	W/m °C
Thermal conductivity of aquifer	2.28	W/m °C
Effective molecular diffusion	$1{\cdot}10^{-10}$	m^2/day

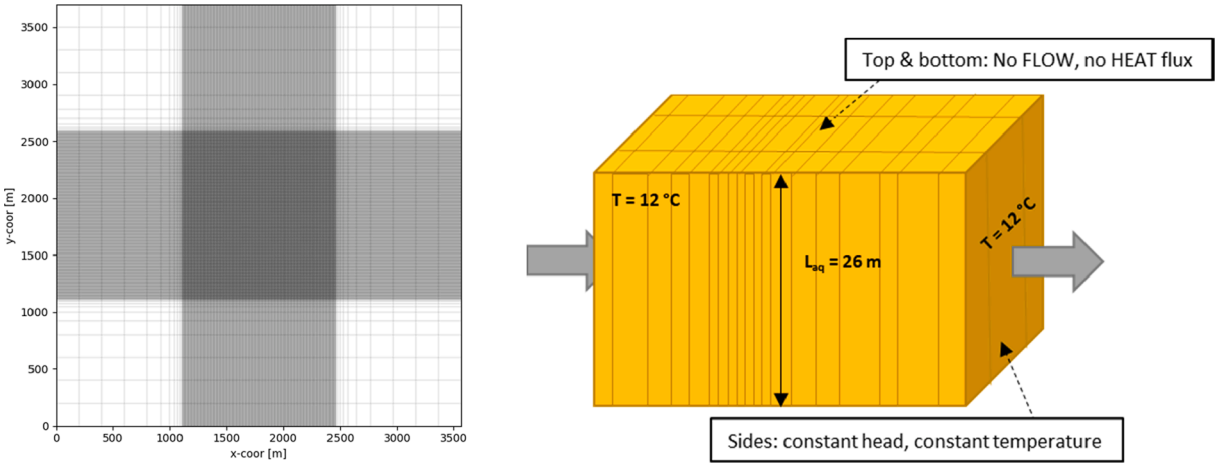

Fig. 10. Left: top view plot of the horizontal discretization. Right: conceptual model of the 3D grid.

automatically takes smaller (internal) time steps if necessary to meet convergence criteria (Courant number < 0.8). The extraction temperatures from the wells are due to the monthly time steps of the groundwater model also constant during each month in the BCI model.

Because ATES systems can have multiple doublets, the average extraction temperature ($T_{extracted}$) of the wells is used as input of the BCI model. The average temperature of the extracted water is calculated for each ATES system at each groundwater model time step using the extraction volume (V) of each well (j) belonging to ATES system (i), following:

$$T_{extracted\_i} = \sum_{j=0}^{m} \frac{T_{extracted\_j} \cdot V_{extracted\_j}}{\sum_{j=0}^{m} V_{extracted\_j}} \tag{27}$$

The groundwater model set-up is the same as the work carried out by [6]. The results of both models showed a good match, which indicates that the model captures the relevant processes and produces realistic results. This allows for comparison of different scenarios with the goal to assess the impact of subsurface interactions on the primary energy use of individual ATES systems. Due to the lack of historical field data, it was not possible calibrate the model to real data. However, the BCI model results were benchmarked to energy demand monitoring data of two existing buildings, and showed a good resemblance, also the energy use of the various components showed a reasonable match, given many uncertainties and gaps in respective data sets.

2.3. Assessment framework

2.3.1. Primary energy use & GHG emission

2.3.1.1. ATES system. The analysis is carried out for the entire simulation period ($t_0 \rightarrow t$). The total electricity used by the heat pump (E_{hp}), dry coolers (E_{dc}), circulation pumps (E_{cp}) and well pumps (E_{wp}) is calculated for each building (i) with an ATES system by:

$$E_{e\_ATES} = E_{hp} + E_{dc} + E_{cp} + E_{wp} = \int_{t_0}^{t} (P_{hp} + P_{dc} + P_{cp} + P_{wp}) dt \tag{28}$$

Similarly the gas use of each ATES system is calculated via:

$$E_{g\_ATES} = E_{boiler} = \int_{t_0}^{t} P_{boiler} dt \tag{29}$$

The total GHG emission is retrieved by calculating the CO_2 emissions of the considered (k) ATES systems:

$$GHG_{ATES} = \sum_{i=1}^{k} (E^{i}_{e\_ATES} \cdot f_{em\_e} + E^{i}_{g\_ATES} \cdot f_{em\_g}) \tag{30}$$

in which f_{em_e} and f_{em_g} are the emissions factors for gas and electricity, and k the number of active ATES systems.

2.3.1.2. Conventional boiler and chiller. Buildings without ATES have a conventional boiler and compression chiller in this model. The total electricity used by the chiller (E_c) and circulation pumps (E_{cp}) is calculated for each building without an ATES system by:

$$E_{e\_conv} = E_c + E_{cp} = \int_{t_0}^{t} (P_c + P_{cp}) dt \tag{31}$$

Similarly the gas use of each building without an ATES system is calculated via:

$$E_{g\_conv} = E_{boiler} = \int_{t_0}^{t} P_{boiler} dt \tag{32}$$

The total GHG emission is retrieved by calculating the CO_2 emissions of the considered buildings:

$$GHG_{conv} = \sum_{n=1}^{l} \left(E_{chiller,h} f_{em\_e} + E_{boiler,h} f_{em\_g} \right) \tag{33}$$

in which f_{em_e} and f_{em_g} are the emissions factors for gas and electricity, and l the number of active conventional systems.

2.3.1.3. Relative change in GHG emissions and primary energy use. The change in primary energy use and GHG emissions as a result of increasing density of ATES wells is compared to the amount of energy use or GHG emissions that would be emitted if the building used conventional heating and cooling system:

$$\Delta GHG_i = \frac{GHG_i}{GHG_{i\_conv}}$$
$$\Delta GHG = \frac{1}{k} \sum_{i=1}^{k} \frac{GHG_i}{GHG_{i\_conv}} \tag{34}$$

This relative change is calculated for each building or for the entire case study area.

2.3.1.4. Emission factors for gas and electricity. For this analysis the Dutch emission factors for 2019 are used (Table 3). The CO_2 emissions per unit electricity use are subjected to change due to the mix of power source contributing to the electricity grid (e.g. coal, solar PV, windmills, nuclear). It is expected that emission factors for electricity of the Dutch grid are decreasing up to almost 50% by 2030, due to an increase of renewable electricity sources, Table 3.

2.3.2. Recovery efficiency of ATES wells

The energy recovery efficiency (η) of the wells of each ATES system over the simulation period is calculated by dividing the extracted amount of thermal energy by the infiltrated amount of thermal energy:

$$\eta(t_0 \rightarrow t) = \frac{E_{out}}{E_{in}} = \frac{\int_{t_0}^{t} (T_{out} - T_{amb}) \cdot c_w \cdot Q_{out} dt}{\int_{t_0}^{t} (T_{in} - T_{amb}) \cdot c_w \cdot Q_{in} dt} = \frac{\Delta \overline{T}_{out} \cdot V_{out}}{\Delta \overline{T}_{in} \cdot V_{in}} \tag{35}$$

The thermal recovery efficiency of all ATES systems in the simulation (η_{tot}) is the average of the individual efficiencies weighted by the individual total storage volume of the wells:

$$\eta_{tot} = \frac{\sum_{i=1}^{k} \eta_i V_i}{\sum_{i=1}^{k} V_i} \tag{36}$$

The recovery efficiencies discussed in this paper are the average efficiencies, averaged for all warm and cold wells of the specific ATES system.

2.3.3. Adoption ratio

As a result of varying well placement policies, the number of buildings with an ATES system and the amount of wells that are being used for ATES systems varies across simulations. This is shown with the adoption ratio of the buildings in the case study area (r_{ATES}), and the adoption ratio of the number of wells (r_w) compared to the needed number of wells for optimal ATES use:

$$r_{ATES} = \frac{k}{k+l}$$
$$r_{well} = \frac{m_{placed}}{m_{needed}} \tag{37}$$

Table 3
Parameters to calculate CO_2 emissions from gas and electricity use.

Name	Value	Description
E_g	**35.17**	Upper calorific value natural gas in MJ/m^3
f_{em_g}	**1.77**	The amount of CO_2-emission (kg) per m^3 gas.
f_{em_e}	*2019:* **0.34***2030:* **0.18**	The amount of CO_2-emission (kg) per KWh$_e$ [37].

2.3.4. Allocated fraction of subsurface space

For various case study areas, the demand for ATES, the settings at street level and the aquifer thickness will differ. The stress on subsurface space will therefore also be different. To allow for proper comparison between simulations of this study, as well as translation of the results provided in this paper, a spatial parameter is calculated. The allocated fraction of subsurface space quantifies the density of the ATES scenario and allows comparison between different model realisations. The allocated fraction of subsurface space is defined as the yearly stored volume of groundwater of all ATES wells, divided by the available aquifer space in the district under consideration:

$$F_s = \frac{\sum_{i=1}^{k} V_i}{L_{aq} A_A} \tag{38}$$

With A_A the ATES area [m^2] and L_{aq} the aquifer thickness [m]. The ATES area (A_A) is defined as the district area (Fig. 11).

2.4. Data and materials

2.4.1. Case study area

The developed methods are applied to the case study area Utrecht, Fig. 11. The city centre is a densely populated/built-up area and contains 26 medium to large (multi utility) buildings with a suitable size and energy profile for ATES. The building characteristics are presented in appendix III.

Because wells cannot be placed beneath buildings or on the train track, available space is limited. In Fig. 11 the building plots are shown for each building. The green area is available to place wells. Around each building plot a buffer is created to correct for the expected extra area that can be used by wells when wells are placed close to the edge of building plots, e.g. in sidewalks. This area is therefore also used to calculate the total available area for ATES (A_a), which is 854,452 m^2 for the case study area Utrecht.

2.4.2. Climate data and reference year

The used climate data to drive the simulations is obtained from the Royal Netherlands Meteorological Institute (KNMI) in the Netherlands. Daily temperature data of the years 2010–2015 of measuring station 'de Bilt' are used, Appendix III. For the initialisation of the climate model (Section 2.2.1) a reference year is used, Appendix III. The reference year is an artificial dataset consisting of separate temperature data fragments and designed as the 'normal' temperature year in the Netherlands and is used in practice to identify the yearly average energy demand and peak load of buildings.

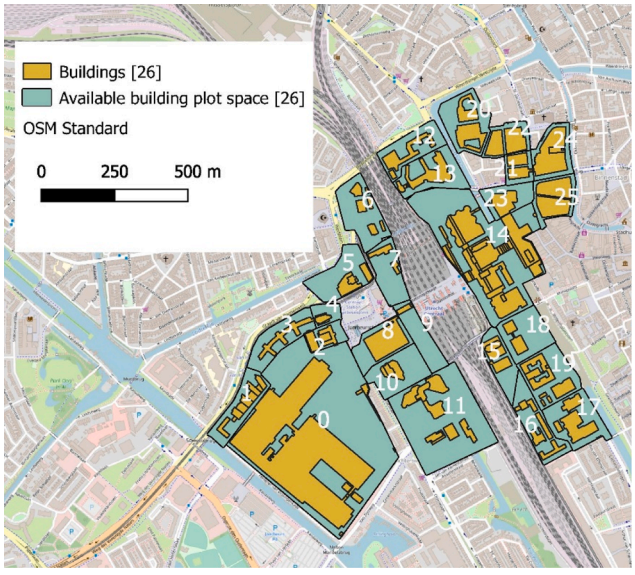

Fig. 11. Case study area Utrecht. The different colours depict the building plot areas and the building itself. The total available building plot space is 854,452 m^2.

2.5. Well placement policy scenarios

In this study, the 'lowest density' placement policy is based on current Dutch design standard ($D_o = 3$, $D_s = 2$) and higher density placement policies follow from Martin Bloemendal et al. [6]. Therefore, D_o is varied as 3, 2.5 or 2, and D_s as 2, 1 or 0.5. Previous research showed that decreasing D_o below 2 leads to a large negative effect on the recovery efficiency, opposite well distance is therefore not tested lower than $D_o = 2$ [6,32]. This results in a total of 9 different well placement policy combinations.

3. Results

3.1. ATES adoption and recovery efficiency

The simulation results illustrate that with applying denser ATES well placement policies (Fig. 12) the number of ATES systems, the individual storage volume and the overall storage volume increases. Consequently, wells of the same type form larger clustered warm and cold volumes, that increasingly adjoin with other clustered storage volumes at their borders.

The densest well placement policy ($D_s = 0.5$ & $D_o = 2$) results in more than double the amount of ATES wells compared to the lowest density placement policy ($D_s = 2$, $D_o = 3$). The stored volume has a strong positive correlation with the allocated fraction of subsurface space (F_s), Table 4. The allocated fraction of subsurface space for the most dense well placement policy is more than twice as large than the most spacious well placement policy.

Decreasing the same well distance (D_s), compared to decreasing the opposite well distance (D_o), has a different effect on well placement and the ability of specific buildings to place wells (Table 4). A smaller D_o has a strong effect on the number of ATES systems that are able to place a minimum of one well doublet, while decreasing D_s has a stronger effect on the number of wells that can be placed for each ATES system. This difference is visible between the $D_s = 2$, $D_o = 2$ and the $D_s = 1$, $D_o = 3$ policy in Table 4. The latter having more total wells on the one hand while these wells are coupled to a smaller amount of buildings. It is therefore beneficial to apply small separation distances between same type of wells in areas with a relatively large share of large buildings in need of many doublets.

Fig. 13 shows the ATES adoption ratio (r_{ATES}), the well adoption ratio (r_{wells}) and the recovery efficiency (η_{th}) for the buildings for 3 well placement policies. This shows that the difference between the two dense well placement policy is relatively small. The highest recovery efficiencies are observed for the most spacious well placement policy and lowest recovery efficiencies are observed for the dense well placement policy. The recovery efficiencies of the buildings, as well as to what extent they are affected by the placement policies varies. These variations are linked to the differences in building size and the associated total storage volume, the proximity of other ATES building plots and the size of the plot, representing how easy it is for buildings to identify suitable well locations under various placement policies. Most buildings do not have a balanced heating and cooling demand (on average 50–100% difference, see table in Appendix III). This has an effect on the heating and cooling loads from the ATES wells, and impacts the energy performance of the cold and warm wells. As most buildings have a higher heating demand, also recovery efficiencies of warm wells are usually higher. However, the results show that this effect is limited (<15%, Appendix IV), which is partly because of the automatic energy balance control of the ATES systems (explained in bullet point 9 in subsection 2.2.1). Buildings 2, 8, 10 and 15 have the lowest recovery

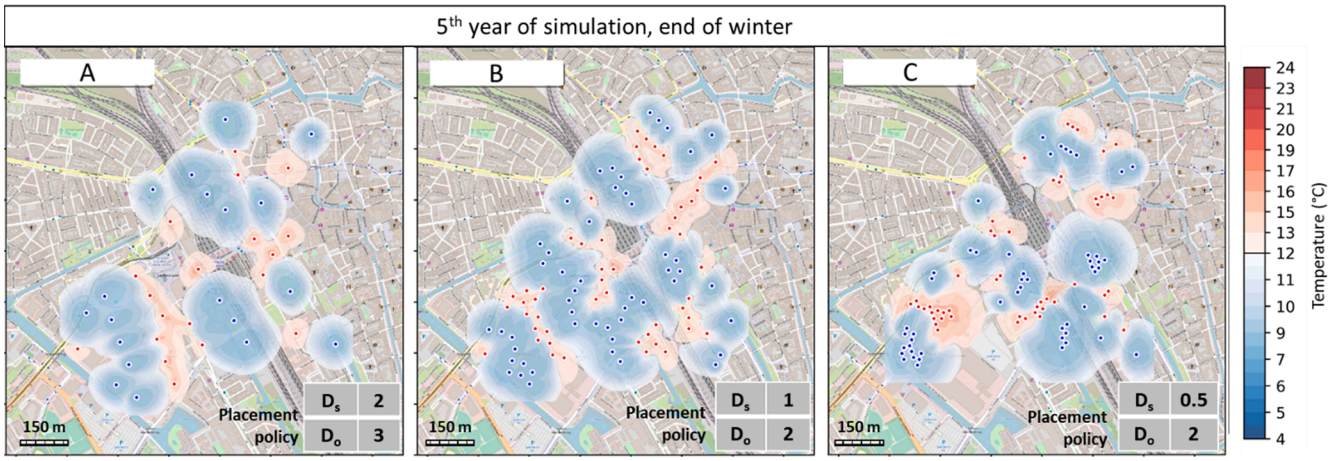

Fig. 12. The effect of different well placement policies based on the relative thermal radius distances between same (D_s) and opposite (D_o) thermal well types on temperature distribution in the storage aquifer in the end of the winter of the 5th year of the simulations for 1 random model realisation for 3 different placement policies. From A-C density well placement density increases with decreasing D_s from 2 to 0.5 times and D_o from 3 to 2 times the thermal radius.

Table 4
Relative amount of buildings with ATES systems (compared to total number of buildings in case study area), placed wells (compared to total well demand), and allocated fraction of subsurface space F_s for the range of policies.

	Policy	Average ATES adoption ratio r_{ATES} (-)	Average Number of wells (m)	Average well adoption ratio *rwell* (-)	Average total storage volume $\sum V$ (Mm^3)	Average case study area F_s (-)
^	$D_S0.5$-D_O2	82%	103	77%	106	110%
more dense	$D_S0.5$-$D_O2.5$	71%	91	72%	93	96%
	$D_S0.5$-D_O3	62%	76	57%	79	84%
	D_S1-D_O2	80%	94	70%	99	102%
	D_S1-$D_O2.5$	69%	82	61%	86	89%
	D_S1-D_O3	60%	70	52%	75	77%
	D_S2-D_O2	71%	58	43%	69	72%
	D_S2-$D_O2.5$	62%	50	37%	60	62%
^	D_S2-D_O3	50%	41	31%	50	52%

efficiencies (in the dense and spacious policy), they are relatively small buildings and located in the centre of the case study area, making them prone to interaction with other buildings, Fig. 11. The large spread in recovery efficiencies across all the model realisations for these buildings presented in Appendix IV illustrates this. While other buildings are limited affected by changes in well placement policies, because they have a large plot to place wells (building 7), are very large (14) or at the boundary of case study area (24). Again, this is illustrated by the limited spread in the efficiencies across all model realisation which are presented in Appendix IV.

Please note that some buildings are missing and some buildings have no result for the low density policy. This is a result of the stochastic well placement approach in the agent based model. Each model realisation is different, also when applying the same well placement policy. This random well placement led to<5 model realisations in which these buildings have an active ATES system for the low density placement policy. 5 realisations or less is considered to be insufficient for representative analysis of the energy use. It concerns buildings 4, 19, 21, 23 in all policies, and buildings 2, 22 and 25 for the most spacious policies. These buildings are therefore excluded from the analysis. The reason for limited ATES adoption for these building is the small available building plot area, which makes it impossible to place an ATES doublet while maintaining the well placement constraints. Even when these buildings are among the first adaptors, the opposite well distance constraint often appeared to be the limiting factor to place an ATES doublet, for both the high as well as low density scenario's. In practice such constraints would be relaxed or well locations would searched somewhat further from the building.

Buildings 0, 1, 11 and 14 have a large building plot and adopt ATES in each model realisation, which means they always have at least one doublet. This does not mean that these buildings are always able to place the designed maximum amount of wells required to fully meet the building demand for all model realisations. For building 0 and 1 this only occurs in about 25% of the realisations.

3.2. Overall GHG emissions

With an increase of the subsurface space use, the average recovery efficiency of all ATES wells decreases, Fig. 14A. This indicates that negative interaction between wells of the opposite type have a stronger effect on the recovery efficiency than the positive interaction between wells of the same type at dense well placement policies (high allocated subsurface fraction, F_s). The decline in recovery efficiency shows a non-linear trend with increasing density, indicating that further increase of ATES density may result in negative recovery efficiencies, i.e. short-circuit flow occurs. Despite the lower average recovery efficiency the

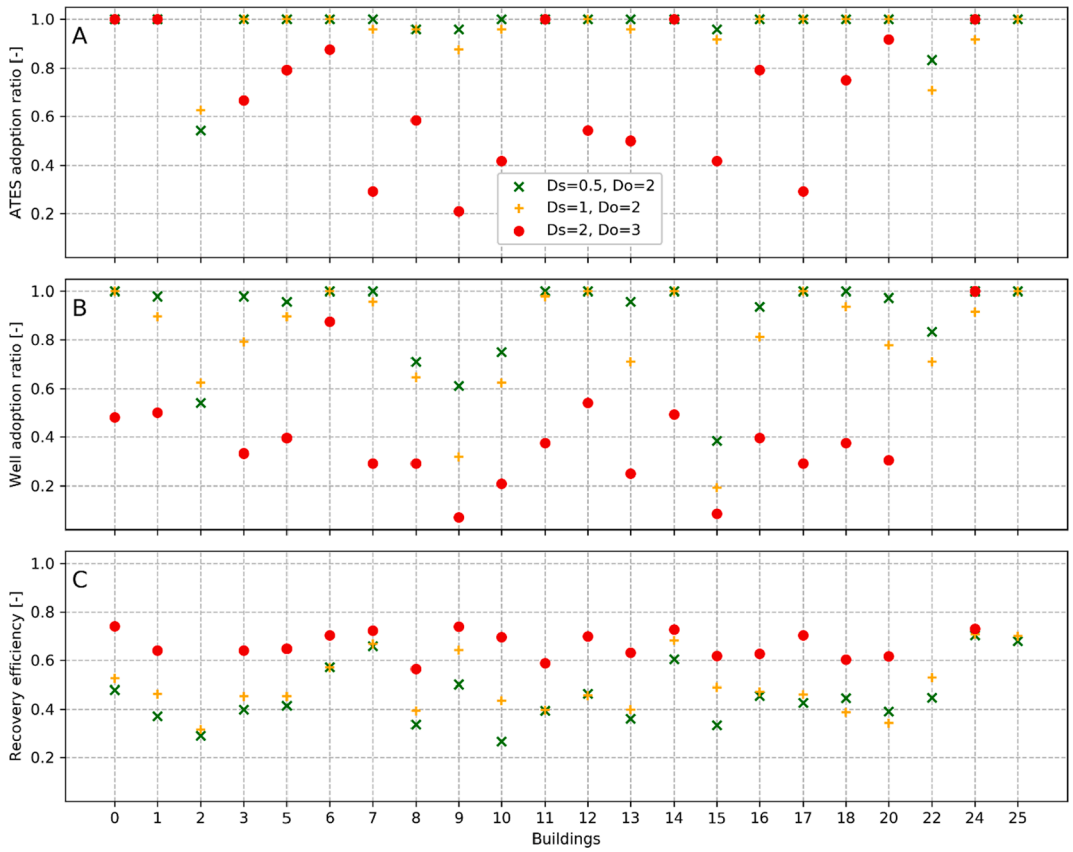

Fig. 13. A: Average ATES adoption ratio (r_{ATES}), B: Average well adoption ratio (r_{wells}) and recovery efficiency (η_{th}) of the individual buildings for the most dense ($D_s = 0.5$, $D_o = 2$), dense ($D_s = 1$, $D_o = 2$) and spacious ($D_s = 2$, $D_o = 3$) well placement policies.

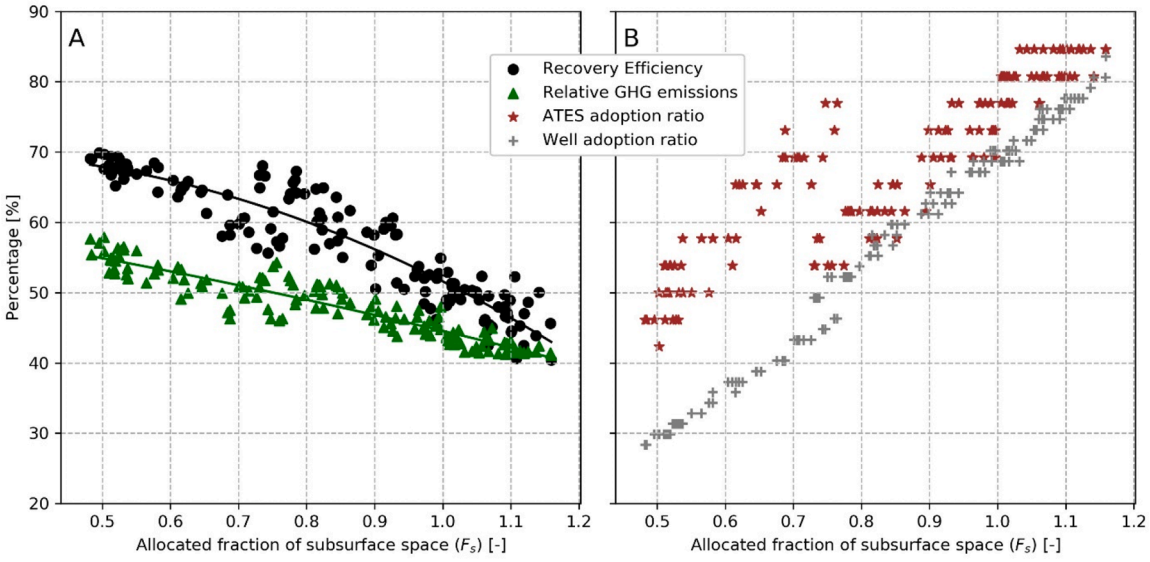

Fig. 14. A: The average recovery efficiency for all wells in different well placement policies and the relative GHG emissions compared to if all buildings used conventional heating and cooling system. B: the ATES adoption ratio, i.e. the percentage of buildings with an ATES system at difference well placement policies. And the average well adoption ratio of all buildings, i.e. the percentage of realised wells at different well placement policies compared to designed amount of wells. Please note that at high density, space in between warm and cold wells can be used twice during a year, at the end of winter it is occupied by the cold well, while at the end of summer it is occupied by the warm well. Hence the allocated surface fraction can be > 1.

total GHG emissions diminish with increasing ATES density, indicating that the increase of buildings with ATES contributes to overall GHG emission reduction, similar to observations by Martin Bloemendal et al. [6].

The ATES adoption ratio is strongly linked to the allocated fraction of subsurface space use, Fig. 14B. The load duration curve (Fig. 6) shows that the first added ATES wells to a building have the largest impact on emission reduction. The simulation results confirm this expected

behaviour: the largest difference in energy savings are initiated at high adoption ratios, i.e. when more buildings have the opportunity to use ATES. This is also illustrated by the contribution of GHG emission by gas and electricity use for the ATES and the conventional situation, presented in Fig. 15. With an increase in number of ATES systems, less conventional systems are operational in the case study area. This results in a mild increase of GHG due to gas and electricity use by ATES buildings (Fig. 15A). While GHG emissions due to electricity and gas use by conventional systems strongly decreases (Fig. 15B). Most buildings do not have their desired amount of wells in the different placement policies, the fact that they have wells already has a large effect on overall emissions.

Fig. 15 also shows that the ratio of GHG emission by electricity/gas for the area as a whole shifts with spacious to dense well placement policy from approximately 50/50 to 70/30. Because electricity use is dominant at dense well placement, future lower emission factors of electricity will even further decrease total CO_2 emissions. In 2030, the GHG emission rate is expected to decrease almost 50% compared to 2019 (Table 3). At high well placement densities this will then result in an even further reduction from 40% emissions in 2019 to only 25% emission in 2030, compared to current emissions by conventional systems.

3.3. The energy performance of individual buildings

The decrease of the overall GHG emissions at high ATES well density is caused by the increase of buildings with ATES and is not related to the energy performance change of individual ATES systems due to a denser well placement policy. To what extent the increased interaction between wells (resulting in the lower recovery efficiencies) at denser well placement policy, affects the primary energy use of individual ATES systems is assessed by evaluating the energy use of each individual building with ATES. The change in gas use, electricity use and GHG emission of each building is calculated relative to the situation with conventional heating and cooling, for a dense and spacious well placement policy (Fig. 16A-B-C). This shows that the gas and electricity use of each building does not change considerably under dense and spacious well placement, Fig. 16 A and B. But because the gas use of a building with ATES is much lower compared to conventional heating and cooling (only 10–20%), the difference in gas use of each building between the dense and spacious well placement policy is still quite large for some buildings, Fig. 16D.

From these results the following observations stand out:

- In general, the average gas use change varies when comparing the dense and spacious well placement policies, while electricity use is less dependent on well placement policy. This is explained by the increase of well doublets per system, which increases the heat pump capacity, and results in less gas is use by the peak boiler, rather than mutual interactions. But there are cases where gas use increases, which is a result of too few warm wells being placed.
- The differences in electricity use is consistently a little bit lower in the dense placement policy. This decrease is caused because more wells can be placed and more cooling is obtained from the ATES rather than the cooling machine. The differences are much smaller than for gas use changes and result in a $< 5\%$ change, predominantly lower in the dense setting, but in one building there is also a larger electricity use.
- The differences in GHG emissions are dominated by the differences in gas use.

The results from Fig. 16 are not conclusive on the effect of mutual interaction on the performance of the ATES system, because the addition of wells mask the impact of interactions on the performance. To discriminate between the implications of the increase of wells and the effect of subsurface interaction, the gas and electricity use of all scenarios for which a building obtains their maximum desired number of wells is presented in Fig. 17. Here, the primary energy use variation is solely influenced by subsurface interaction. The energy use change at increasing aquifer utilization levels is shown compared to the energy use at the lowest aquifer utilization level for which each building has obtained their maximum number of wells. Negative impact at aquifer utilization levels up to 80% is limited to max 5% for both gas and electricity use. At higher levels, some building observe a gas use or electricity use increase of maximally 15%. However, this is only limited to a few buildings. The maximum and minimum change increases with higher well placement density. The average change of all buildings however is limited to $< 5\%$ at the highest densities for both electricity

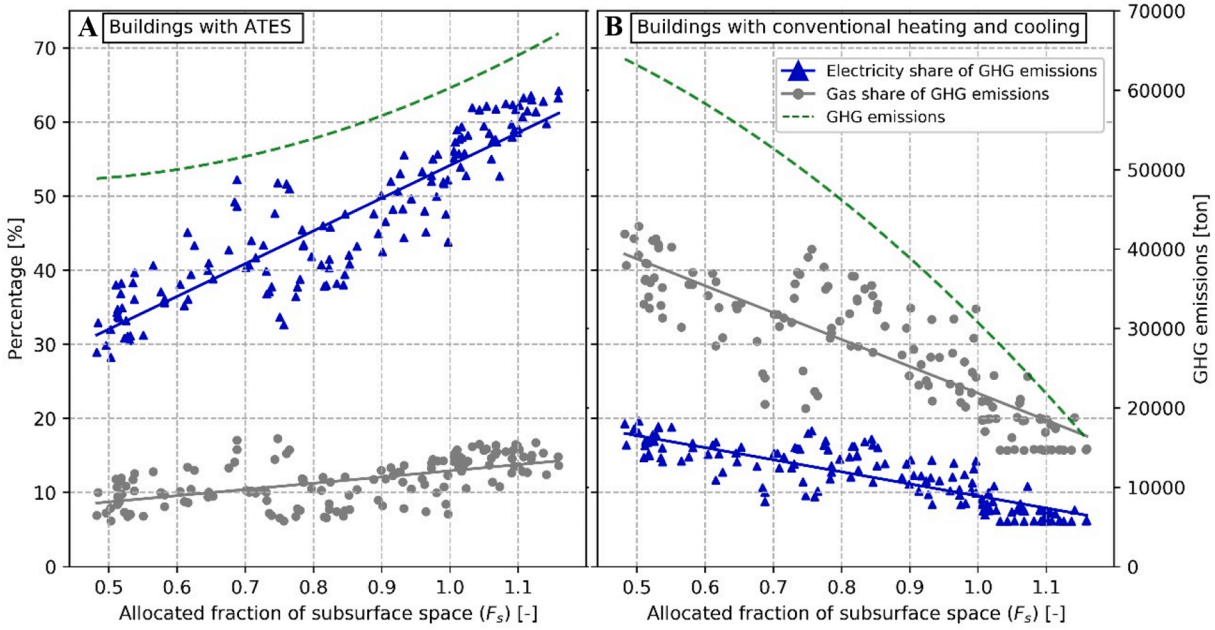

Fig. 15. Share of total GHG emissions due to buildings with an ATES systems (left) and building with conventional buildings (right). With higher allocated fraction of subsurface space (F_s) the share of emitted GHG emissions increases for ATES and decreases for conventional buildings.

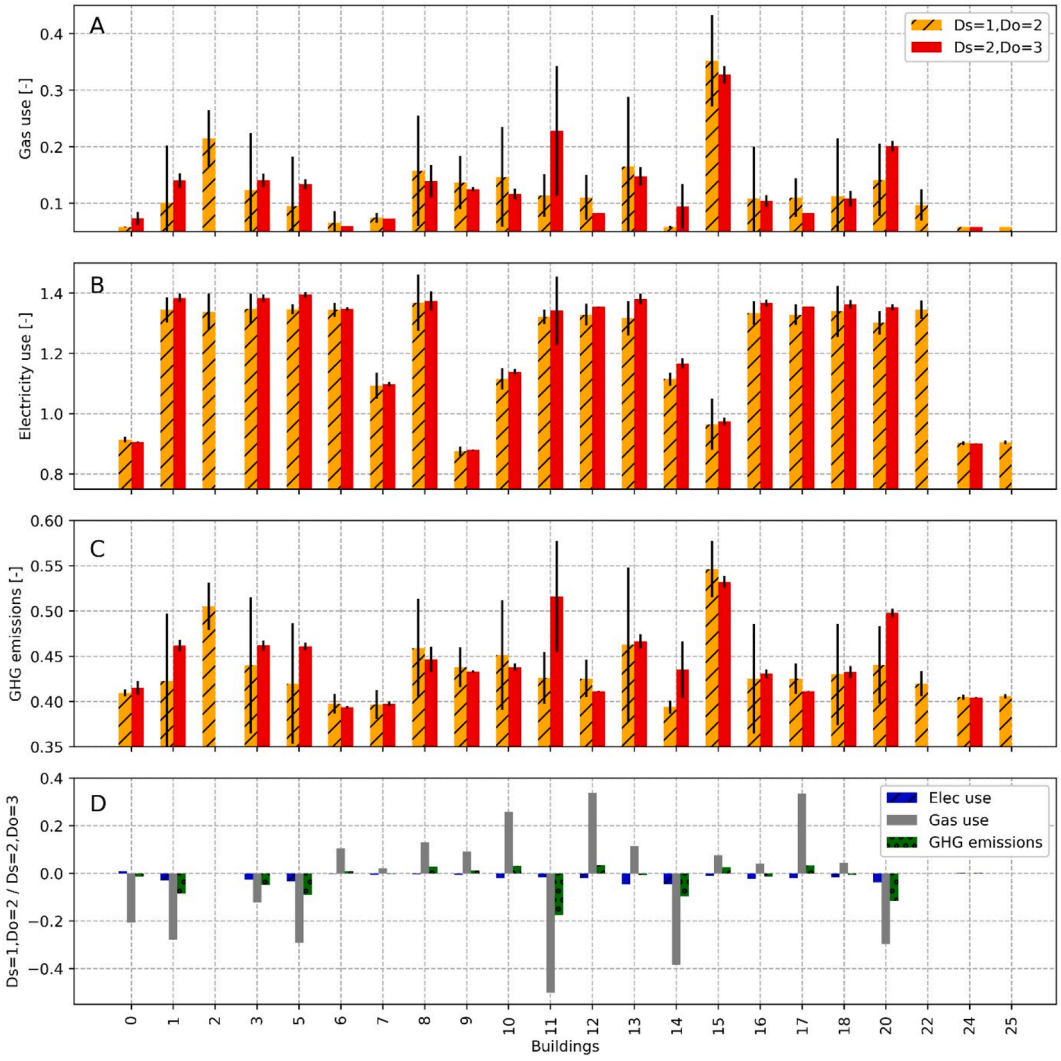

Fig. 16. Gas (A) and Electricity (B) use and GHG emissions (C) for the buildings with an ATES system relative to conventional systems, compared between spacious ($D_s = 2$, $D_o = 3$) and dense ($D_s = 1$,$D_o = 2$) well placement scenario. The error bars represents 2 standard deviations. D: the average relative change in electricity and gas use and GHG emissions for each building between high and low density placement scenario's. Please note that the buildings 2, 22 and 25 do not have ATES wells in the spacious well placement scenario.

and gas use (solid line, Fig. 17).

Fig. 17 shows that the effect of subsurface interaction at increasing aquifer utilization varies strongly for each individual building, and is thus affected by local conditions. Therefore, 5 buildings that had their maximum required wells in most of the model realisations across all placement policies are showed in Fig. 18 to assess what conditions cause this variability. Please note that:

- Buildings 6 and 7 and their neighbouring buildings have much more space available to identify well locations, see Fig. 11.
- Buildings 6, 12 and 17 have the same function and specific energy use and therefore respond similarly, especially in the electricity use. They have a strongly imbalanced heating and cooling demand, heating demand is larger, see Appendix III.
- Building 7 is much larger than the other buildings and has a larger cooling demand than buildings 6, 12 and 17, see Appendix III.
- Building 24 has a balanced heating and cooling demand (For details, see Appendix III)

Fig. 18 shows the gas use, electricity use and GHG emissions as a function of the allocated subsurface fraction for these 5 buildings. For all 5 buildings it is concluded that both gas and electricity use is not much affected by subsurface interaction with allocated subsurface fraction up to 0.8. At higher density placement policies, the smaller buildings may suffer from a considerable amount of gas use increase, max 9%. For all 5 buildings, the electricity use varies max. 5% for $F_s < 0.8$, and for the smaller buildings, the electricity use does not vary >2% up to 0.9 allocated aquifer fraction. Building 7 has, a much lower electricity use compared to the other buildings (around 1.1 vs. 1.35), due to a relatively large cooling demand. But as a result it is also more sensitive for mutual interactions at higher allocated subsurface fractions. Building 24 with the balanced heating and cooling demand doesn't seem to suffer from the subsurface interaction. This may be caused by the fact that 1) it is on the boundary of the study site and 2) due to its' high cooling demand, warm wells are always fully charged and therefore gas use is not much affected. Please note that for the buildings with an imbalanced heating and cooling demand the correction for the imbalance usually lags behind by a year, which is also the case in practice (see step 9 in the operation dynamics description in section 2.2.1). Building 7 (in the middle of the study area), which also has a higher cooling demand compared to the other 3 buildings with a stronger imbalance towards larger heating demand, also shows less sensitivity for gas use due to interactions.

These results show that ATES adoption can be accommodated in areas up to an aquifer allocated subsurface fraction of 80%, without

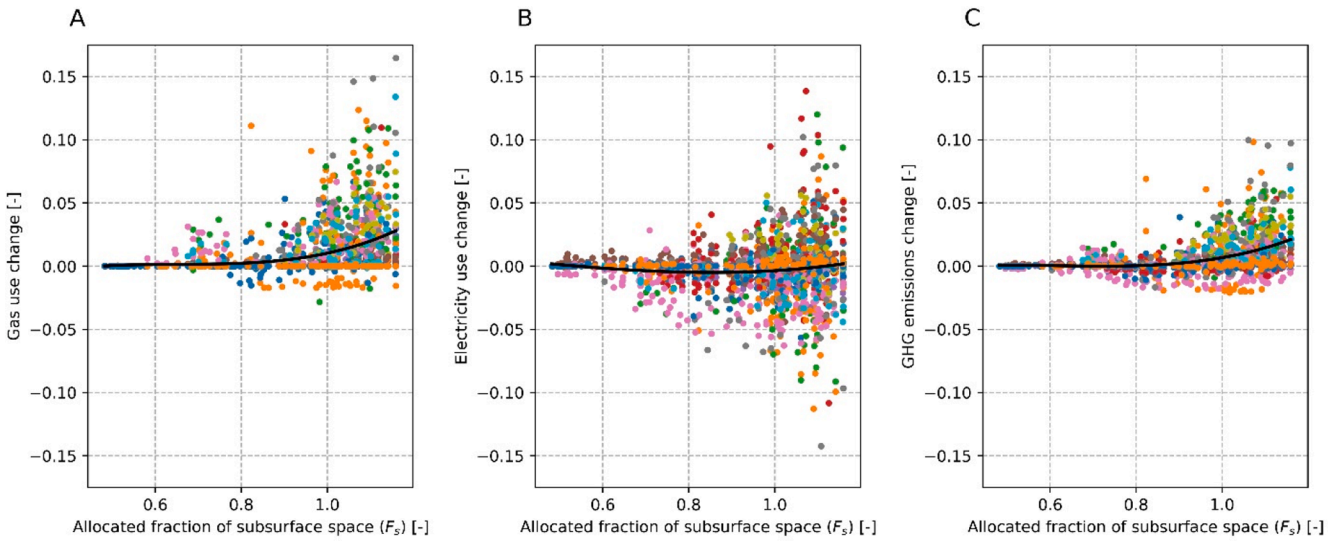

Fig. 17. Gas use, electricity use and GHG emissions change for individual ATES systems in different model realisations due to increasing levels of aquifer utilization (F_s) compared to the lowest aquifer utilization model run that resulted in the maximum number of desired wells for each individual ATES system / building. The solid line indicates the average change of the ATES systems at given F_s.

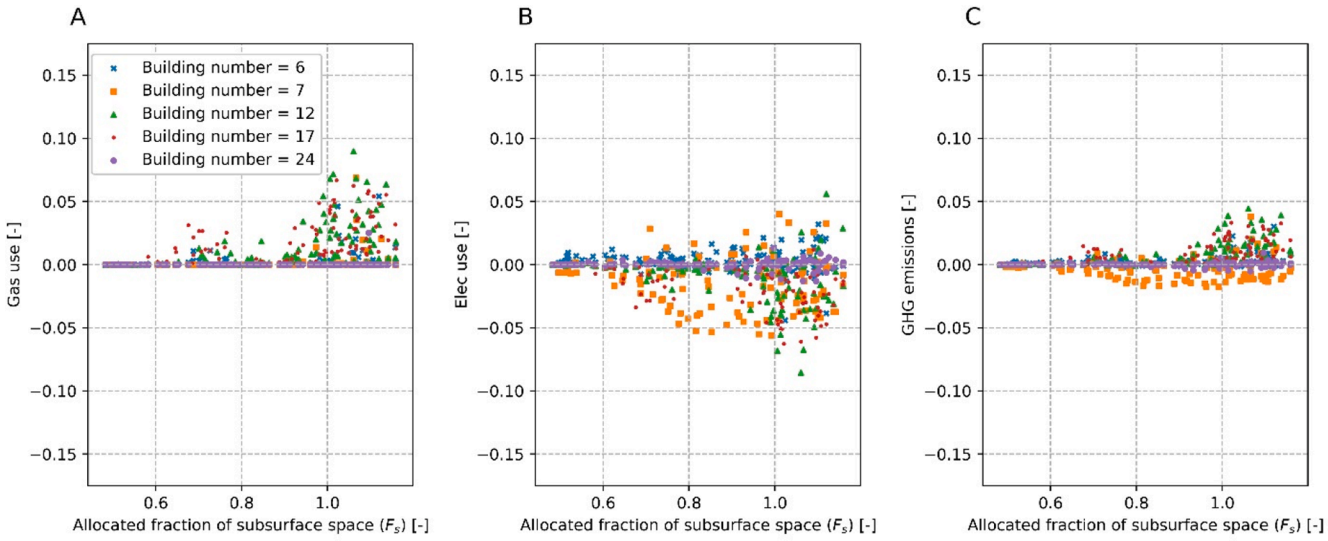

Fig. 18. Relative change in gas (A) and electricity (B) use compared to conventional systems for 5 buildings which have the maximum number of ATES wells for all model realisations. The differences in energy use are therefore only caused by mutual interactions.

considerable negative impact on the performance of individual ATES systems. These results are in correspondence with the earlier work of Martin Bloemendal et al. [6] and allow for higher aquifer utilisation than current practice for ATES planning does (i.e. 25–40%, Martin Bloemendal et al. [6]; Martin Bloemendal et al. [7]. Additionally, the results indicate that buildings with a balanced heating and cooling demand suffer less from mutual interactions.

4. Discussion

4.1. Permit vs. real storage volume: which thermal radius to use for well placement?

In the simulations in this study, the thermal radius used for well placement is representative for the actual average thermal radius that develops for the ATES systems in the simulation. The maximal yearly thermal radius varies slightly between consecutive years, due to variations in outside air temperature, like they would also in practice. However, the thermal radius used for planning in practice, is based on the maximal storage volume requested in the permit. This is the allowed storage volume in case of an extremely warm summer, or extremely cold winter. As a design value, the permitted capacity is often chosen to be 1.5 times the expected yearly capacity, while in practice monitoring data shows that the permitted total volume is >2 times larger than the actual average storage volume [33–34]. Hence, applying the permit volume to calculate the maximum thermal radii for well placement will overestimate the thermal radii, and thus result in underutilisation of aquifer space. Therefore, it is recommended to use the thermal radius resulting from the average expected storage volume for the well placement (or adapt the placement rules to account for the safety factor in permit capacity). This can be done by requesting both the estimated average and maximum storage volume for the new ATES system, when applying for a permit. The permit application of course has to be checked to prevent that the maximum yearly storage volume is submitted as the average storage volume, as this is preferential for the ATES owner.

In the Netherlands, local authorities also apply the "use it, or lose it" rule. When permit capacity is not used for several years, the allowed storage volume in their permit is reduced. This creates space for new ATES initiatives. However, wells of the existing ATES systems will not be relocated when this happens. Therefore, it is key for local authorities to prevent the use of overestimated storage volumes in the ATES permit, to enable correct well placement and optimize utilization of subsurface space.

Given the large uncertainties in expected energy use of new buildings and tendency for individual ATES owners to request for larger storage capacity than they expect to use, it is logical to tend towards more dense well placement distances: <0.5 for D_s and < 2 for D_o.

Another aspect that may be of influence on the yearly storage volume, is the temperature of the warm and cold well. If for future BCI systems, larger temperature differences between the warm and cold well can be obtained, the storage volume reduces, which may be an efficient way to improve accommodation of ATES system. However, with smaller storage volumes energy losses increase [21]. And possibly, also the sensitivity of lower recovery efficiency on total primary energy use could increase.

4.2. Difference between gross and net storage volume

The total (gross) storage volume is used for the thermal radius used for well placement. But, during fall and spring ATES systems change flow direction regularly to supply both heating and cooling [35]. These pumping operations contribute to the yearly (gross) storage volume, but the (net) storage volume in one well is smaller and results in a smaller thermal radius, than expected. Also during these seasons, thermal radius is not at its largest, hence, these short-term injections and extraction do not result in mutual interaction. This explains why the monthly time steps for the groundwater model works well with the hourly BCI time steps for the simulations in this study (see section 2.2.3). In this study, the average difference between gross and net storage volume was about 15%, while in practice this may go up to almost 30% [35]. In the simulations this effect was taken into account as a result of the longer groundwater model time step. Therefore, the distances identified are still applicable for moderate climatic zones such as in the Netherlands. In climatic zones with a stronger pronounced heating and cooling season, resulting in a small difference between gross and net storage volume, ATES systems performance may react stronger to dense well placement setting and well distances may need to be somewhat larger. At the same time, in climatic zones that have a heating and cooling season that is even less pronounced compared to the Dutch situation, the well distances may be reduced. This may also be the case for the Netherlands, as the simulated difference between gross and net storage volume is lower than in practice, according to the observations in M Bloemendal et al. [35].

4.3. Placement rules in practice

4.3.1. Placement rules applied to individual ATES building plots

In the simulations, same placement rules apply to all wells, also for the wells of one individual ATES system. However, in practice ATES designers are more flexible with placement of the wells of one individual system. The results of the most dense placement policies are representative for these conditions: in practice wells of the same type are often placed at distance $0.5 \cdot R_{th}$, or even shorter. The opposite well types distance is usually not smaller than $2 \cdot R_{th}$. This means that in practice wells of one individual ATES system are currently in practice already placed using the dense placement policy. When there are few buildings with many doublets, a spacious well placement policy would in practice look like the dense well placement policy as it is simulated in this study. However, in the study site there are many buildings (26) of which 9 and 10 have respectively 1 or 2 doublets, 7 buildings require more doublets. Hence, the results are representative for area's with many buildings with a limited number of required doublets (1 or 2). For areas with fewer, but larger buildings with many doublet, the spacious well placement may differ less from the dense placement policy than is identified in this study.

For the dense well placement scenario, it is reasonable to expect that this artefact results in smaller thermal influence outside the buildings plot for a given amount of wells, or similar thermal influence for more wells placed. Which in both cases is positive for the overall performance. The results of this study are "worst-case" in that sense.

Furthermore, it would be beneficial from a practical point of view, if there is no need to make a distinction between how wells are placed relative to each other, within an ATES system, or between different ATES systems. Therefore, it is logical to stay on the small side for the distance multipliers: <0.5 for D_s and ~ 2 for D_o.

4.3.2. Wells in public space

When it is not possible to find an optimal well location, or a well location at all, ATES wells are often placed in the public space around the associated building. In the Netherlands, the extent to which municipalities facilitate this, differs. In this study, the building plot boundaries are set in such a way that adjacent sidewalks, squares and parks are included, to allow for well locations in public space. Some of the buildings in the study area benefit greatly from this, while others don't. It is not analysed to what extend well locations indeed end up in public space. However, the large differences in ATES adoption ratio and the resulting GHG emissions reductions at denser well placement policies indicate a great benefit of allowing ATES system designers to place wells in public space when individual building plot space is limiting.

4.4. Comparison to other ATES design and sustainable energy systems

As is common, the use of a conventional boiler and compression chiller was used in this study as a reference for conventional building climate control. But they cannot be evaluated as a sustainable alternative for ATES. This study would therefore benefit from a follow-up analysis to also asses alternative sustainable heating/cooling systems. Furthermore, all ATES systems in this study have the exact same BCI design and control, following the basis of the Dutch standard [19]. In practice however, this standard is always tuned to specific building requirements, which may (considerably) affect behaviour and performance of the BCI system. For example, the ATES system may be designed to exclude the use of gas (monovalent ATES system), meaning that the BCI is equipped with a heat pump at the required maximum heating capacity and no peak boiler. Dense and spacious placement policies are used to simulate the use of monovalent ATES systems in this case study area, see Fig. 6. As a result the well placement dynamics change: due to the increased peak demand, the total capacity (m^3/h) of the ATES wells needs to be increased. Consequently, the number of wells required for a given ATES system approximately doubles. While at the same time, the required storage volume increases with only about 20%. As a result, more wells with relatively small thermal radii need to placed. The total combined thermal radius of the wells only increases with 20%. Table 5 confirms this change in "well placement behaviour", as many more wells are placed under the same placement policies. Due to the smaller thermal radii it is easier to find well locations, also at dense placement policies. As a results the well adoption ratio is not much affected, despite the increased number of wells. For example: a required 250 000 m^3 storage volume in a 25 m thick aquifer for a bivalent ATES system has a thermal radius of 70, requiring $<$ 35 m distance to same type of wells. When two of these wells are cluster the total thermal radius is 100 m. If this is now a monovalent system, each well needs $250\,000 \times 1.2 / 2 = 150\,000$ m^3, resulting in an individual thermal radius of 55 m and a combined thermal radius (now of 4 wells) of 105 m.

Fig. 19 shows the recovery efficiency, GHG emissions and energy use for the bivalent and monovalent scenarios. Please note that there is still gas use in the monovalent results because ATES systems which do not

Table 5
Simulation results meta data: increase of active ATES systems, number of wells and aquifer utilization for monovalent ATES compared to the bivalent simulation results for dense ($D_s = 1, D_o = 2$) and spacious ($D_s = 2, D_o = 3$) well placement policies.

	Active ATES systems [-]		Number of wells [-]		Well adoption ratio [-]		Allocated aquifer fraction (F_s) [-]	
	dense	spacious	dense	spacious	dense	spacious	dense	spacious
Bivalent	20.8	13.0	93.9	41.1	0.70	0.31	1.02	0.52
Monovalent	23.5	20.3	194.5	82.8	0.72	0.30	1.54	0.93

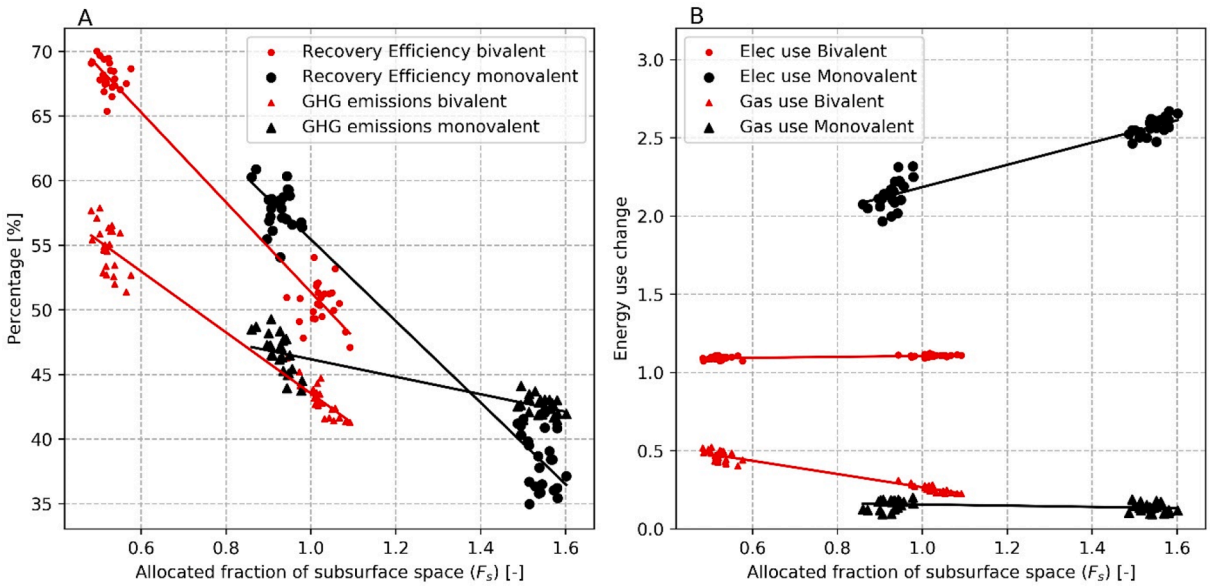

Fig. 19. Monovalent and bivalent simulation results. A: recovery efficiency and GHG emissions reduction. B: electricity and gas use.

receive the desired number of wells, or no wells at all, still need a(n additional) source of heat to meet their heating demand. This is again done with gas fired boilers. For the same placement rules, more wells can be placed, which results in a higher allocated fraction of subsurface space, F_s. Compared to the bivalent ATES concept, the average recovery efficiency is affected less for similar subsurface space use, which is due to the smaller radii of the stored thermal volumes which makes their placement easier and thus results in less influence by other wells. The recovery efficiency has the same trend towards higher allocated subsurface fractions (same slope). The GHG emissions show a different trend, because monovalent systems in principle do not use gas, the GHG emissions mainly depend on electricity, and are as a result less sensitive. The GHG emission reductions are smaller compared to bivalent systems, this is because there is little gas use in the monovalent cases and due to the large emission factors in the current electricity grid mix in the Netherlands, which is likely to decrease. Whereas the electricity use does

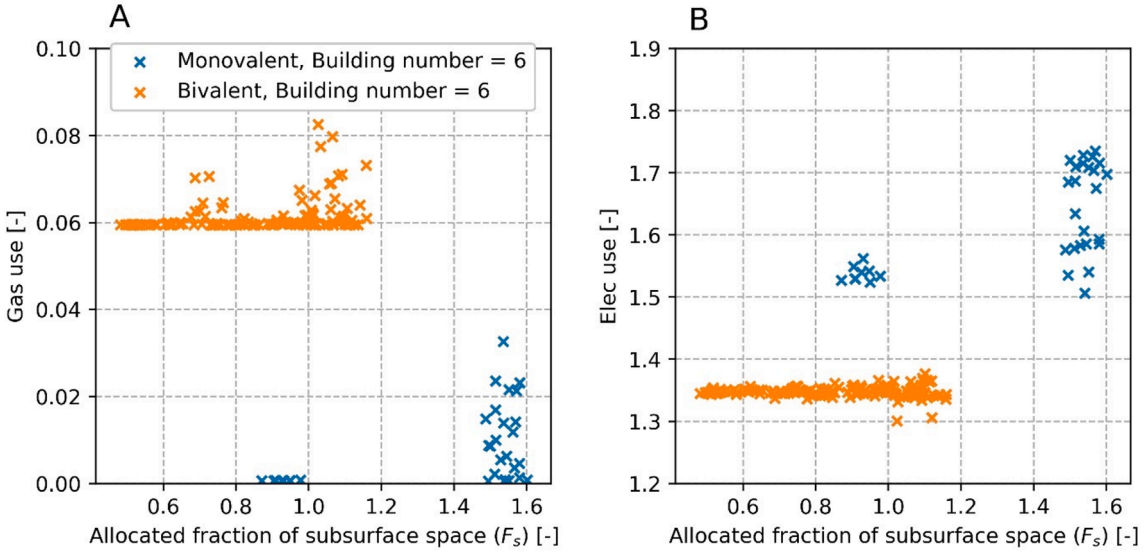

Fig. 20. Relative change in gas (A) and electricity (B) use compared to conventional systems for building 6 with the maximum number of ATES wells for all monovalent and bivalent model realisations. The differences in energy use are therefore only caused by mutual interactions.

not change much at higher densities in the bivalent case, in the monovalent scenario's this increases significant, hence the less sensitive trend in the GHG emissions.

Therefore, also for the monovalent ATES design decreasing the well distance also helps for better utilisation of subsurface space and overall reduction of GHG emissions. Again also the gas and electricity use of individual buildings are analysed for the model realisations where they have the maximum desired wells installed, unfortunately only one of the previous 5 now has model realisations with all required wells in the low density scenario. Fig. 20 shows the gas and electricity use as a function of the allocated subsurface fraction for building 6. Despite that only one building has its maximum desired wells it is still possible to derive how interaction due to increased subsurface space use affects the performance of individual monovalent ATES systems. Please note that the gas use is included because the model automatically provides heat with gas when the ATES system is not possible to provide the required heating. But in the situation that all desired well are installed, the building would not have a gas boiler. Therefore, the gas use in Fig. 20 represents to what extent the ATES system is not able to provide the required heating due to subsurface interactions. For the low density scenario there is no gas use so the ATES system can always provide heating demand. At the dense well placement policy interactions result in poorer performance, resulting in some cases a couple of percent of the heating demand not able to be fulfilled, however, most of the cases<1%. Also the electricity use is affected by a couple of percent. Because it is only one building it is hard to draw strong conclusions. Nevertheless, the results are similar with the bivalent systems for building 6. There is a small impact due to mutual interaction, only where bivalent systems sometimes also have a positive effect of mutual interaction on total energy use, the monovalent systems only have higher energy use due to mutual interactions.

5. Conclusions

The results of this study show that the change in primary energy use for individual ATES systems under denser well placement policies results in two main aspects:

1) Buildings can place more wells, therefore this leads to increased heat pump electricity use and less boiler gas use. Even when buildings only have a part of their required ATES well capacity installed, their GHG emissions reduce considerably. The largest effect on GHG emissions reductions is observed for the first added ATES well doublet (Fig. 16), due to the shape of the load duration curve (Fig. 6).
2) ATES wells have lower recovery efficiencies. This, however, has negligible effect on the combined electricity consumption of the heat pump and well pumps and peak boiler gas use at allocated subsurface fraction < 0.8. At higher density there may be a considerable negative effect on peak boiler gas use consumption for relative small buildings as well as a $> 5\%$ change in electricity use (increase or decrease) for buildings with a large cooling demand.

Furthermore, the overall results for this study confirm earlier work that denser placement policies lead to an overall decrease of GHG emissions due to larger adoption rates of ATES technology.

5.1. Implications for practice:

By increasing well placement density, first adopters who have installed the designed/desired amount of wells may suffer some percentage gas use increase due to lower ATES performance caused by increased subsurface interaction. However, the "first ATES well doublet effect" results in much larger gas use reduction for late adopters than it results in a gas use increase for first adopters. Therefore, it is important to either limit the number of wells for first adopters, or better: ensure in their permit conditions, that they allow future neighbours to affect their well efficiency in a controlled way. For first adopters it is more beneficial to have their desired number of wells, which might perform a little less once the area is filled up with ATES systems, rather than having a limited amount of wells. For late adopters a more dense well placement setting is always beneficial. Even if this enables them to place only one ATES doublet of many required, a considerable emission reductions can be achieved.

The optimal well placement policy is: 0.5 for D_s and 2 for D_o. And, if possible, it is more preferable to use smaller multipliers than larger, especially for the same well types. The storage volume used to determine the thermal radius for well placement should be the average yearly storage volume, not the maximum. Local authorities should carefully verify permit storage volumes used for planning of ATES wells, to prevent unnecessary claims on subsurface space due to ATES permits with too large maximum and/or average yearly storage volume.

5.2. Further research:

The monovalent ATES concept leads to more flexible well placement conditions, therefore a higher allocated fraction of subsurface space and increase of GHG emissions reduction. The performance of individual monovalent ATES systems is a bit more sensitive for mutual interaction, than bivalent ATES systems. But the effect of mutual interaction on different ATES systems design (e.g. monovalent) should be further investigated as the results in this study are not conclusive.

The results indicate that ATES systems with a balanced heating and cooling demand are less sensitive for mutual interactions. Which implies the need for stronger anticipation on imbalances, e.g. using predictive control to restore the energy balance in time, rather than lag behind a year like is common in practice. To what extend this would indeed reduce sensitivity, and which methods can be used, is still to be determined.

CRediT authorship contribution statement

Stijn Beernink: Methodology, Software, Validation, Investigation, Visualization, Writing – original draft, Writing – review & editing. **Martin Bloemendal:** Conceptualization, Methodology, Software, Investigation, Supervision, Funding acquisition, Writing – original draft, Writing – review & editing. **Rob Kleinlugtenbelt:** Methodology, Software, Writing – review & editing. **Niels Hartog:** Writing – review & editing.

Declaration of Competing Interest

The authors declare that they have no known competing financial interests or personal relationships that could have appeared to influence the work reported in this paper.

Acknowledgements

This research was funded by TKI (Topconsortia voor Kennis en Innovatie), BodemenergieNL (kennisplatform bodemenergie), KIBO (Kennis en Innovatieprogramma Bodem en Ondergrond), Province and Municipality of Utrecht and NWO (grant number 408-13-030). The authors thank dr. Marc Jaxa-Rozen for his help with setting up the agent based model and the TKI project partners for their input on the simulation results: Johan Valstar of Deltares, Marian van Asten and Marlous van der Meer of the Province of Utrecht, Harry Boerma of the Municipality of Utrecht and Jan Frank Mars of the Ministry of Infrastructure and Environment. Furthermore we thank the editor and 4 anonymous reviewers for their valuable suggestions for improvements.

Appendix A. Supplementary data

Supplementary data to this article can be found online at https://doi.org/10.1016/j.apenergy.2022.118587.

References

[1] IEA, IRENA, & REN21. (2020). Renewable Energy Policies in a Time of Transition - Heating and Cooling (ISBN 978-92-9260-289-5). Retrieved from https://www.iea.org/.

[2] Fleuchaus P, Godschalk B, Stober I, Blum P. Worldwide application of aquifer thermal energy storage – A review. Renew Sustain Energy Rev 2018;94:861–76. https://doi.org/10.1016/j.rser.2018.06.057.

[3] Bloemendal M, Olsthoorn T, van de Ven F. Combining climatic and geo-hydrological preconditions as a method to determine world potential for aquifer thermal energy storage. Sci Total Environ 2015;538:621–33. https://doi.org/10.1016/j.scitotenv.2015.07.084.

[4] Stemmle R, Blum P, Schüppler S, Fleuchaus P, Limoges M, Bayer P, et al. Environmental impacts of aquifer thermal energy storage (ATES). Renew Sustain Energy Rev 2021;151:111560. https://doi.org/10.1016/j.rser.2021.111560.

[5] Tomasetta C, van Ree CCDF, Griffioen J. Life Cycle Analysis of Underground Thermal Energy Storage 2015;Vol. 2:1213–7.

[6] Bloemendal M, Jaxa-Rozen M, Olsthoorn T. Methods for planning of ATES systems. Appl Energy 2018;216:534–57. https://doi.org/10.1016/j.apenergy.2018.02.068.

[7] Bloemendal M, Olsthoorn T, Boons F. How to achieve optimal and sustainable use of the subsurface for Aquifer Thermal Energy Storage. Energy policy 2014;66:104–14. https://doi.org/10.1016/j.enpol.2013.11.034.

[8] Hardin G. tragedy of the commons. Science 1968;162:1243–8. https://doi.org/10.1126/science.162.3859.1243.

[9] Bloemendal M, Jaxa-Rozen M, Rostampour V. Use it or lose it, adaptive ATES planning. Paper presented at the 12th IEA Heat Pump conference Rotterdam. 2017.

[10] Jaxa-Rozen M, Kwakkel JH, Bloemendal M. The Adoption and Diffusion of Common-Pool Resource-Dependent Technologies: The Case of Aquifer Thermal Energy Storage Systems. Portland: Paper presented at the PICMET; 2015.

[11] Rostampour V, Jaxa-Rozen M, Bloemendal M, Kwakkel J, Keviczky T. Aquifer Thermal Energy Storage (ATES) smart grids: Large-scale seasonal energy storage as a distributed energy management solution. Appl Energy 2019;242:624–39. https://doi.org/10.1016/j.apenergy.2019.03.110.

[12] Hähnlein S, Bayer P, Ferguson G, Blum P. Sustainability and policy for the thermal use of shallow geothermal energy. Energy policy 2013;59:914–25. https://doi.org/10.1016/j.enpol.2013.04.040.

[13] Sommer W, Valstar J, Leusbrock I, Grotenhuis T, Rijnaarts H. Optimization and spatial pattern of large-scale aquifer thermal energy storage. Appl Energy 2015;137:322–37. https://doi.org/10.1016/j.apenergy.2014.10.019.

[14] Jaxa-Rozen M, Kwakkel JH, Bloemendal M. A coupled simulation architecture for agent-based/geohydrological modelling with NetLogo and MODFLOW. Environ Modell Software 2019;115:19–37. https://doi.org/10.1016/j.envsoft.2019.01.020.

[15] Perez F, Granger BE, Hunter JD. Python: An Ecosystem for Scientific Computing. Comput Sci Eng 2011;13(2):13–21. https://doi.org/10.1109/MCSE.2010.119.

[16] Harbaugh, A. W., Banta, E. R., Hill, M. C., & McDonald, M. G. (2000). Modflow-2000, the U.S. Geological survey modular ground-water model—user guide to modularization concepts and the ground-water flow process Virginia: US Geological Survey. Retrieved from https://www.usgs.gov/mission-areas/water-resources/science/modflow-and-related-programs.

[17] Zheng, C., & Wang, P. (1999). MT3DMS v5.3. A modular three-dimensional multispecies transport model for simulation of advection, dispersion and chemical reactions of contaminants in groundwater systems. Documentation and User's Guide. Retrieved from https://hdl.handle.net/11681/4734.

[18] Wilensky, U. (1999). NetLogo. Evanston, IL.: Center for Connected Learning and Computer-Based Modeling, Northwestern University, . Retrieved from http://ccl.northwestern.edu/netlogo/.

[19] ISSO. ISSO-publicatie 39 Energiecentrale met warmte en koude opslag (WKO). Rotterdam: ISSO; 2017.

[20] KvINL. (2017). BRL 6000-21/00 - Ontwerpen en installeren van energiecentrales van bodemenergiesystemen en het beheren van bodemenergiesystemen. In. Zoetermeer: KvINL.

[21] Bloemendal M, Hartog N. Analysis of the impact of storage conditions on the thermal recovery efficiency of low-temperature ATES systems. Geothermics 2018;17:306–19. https://doi.org/10.1016/j.geothermics.2017.10.009.

[22] Sommer WT, Doornenbal PJ, Drijver BC, van Gaans PFM, Leusbrock I, Grotenhuis JTC, et al. Thermal performance and heat transport in aquifer thermal energy storage. Hydrogeol J 2014;22(1):263–79. https://doi.org/10.1007/s10040-013-1066-0.

[23] McDonald MG, Harbaugh AW. *A modular three-dimensional finite-difference ground-water flow model* (06–A1). Retrieved from 1988. http://pubs.er.usgs.gov/publication/twri06A1.

[24] Hecht-Mendez J, Molina-Giraldo N, Blum P, Bayer P. Evaluating MT3DMS for Heat Transport Simulation of Closed Geothermal Systems. Ground Water 2010;48(5):741–56. https://doi.org/10.1111/j.1745-6584.2010.00678.x.

[25] Langevin, C. D., Thorne, D. T., Dausman, A. M., Sukop, M. C., & Guo, W. (2008). SEAWAT Version 4: A computer program for simulation of multi-Species Solute and heat transport. Retrieved from Reston, Virginia: https://www.usgs.gov/mission-areas/water-resources/science/modflow-and-related-programs.

[26] Bakker M, Post V, Langevin CD, Hughes JD, White JT, Starn JJ, et al. Scripting MODFLOW Model Development Using Python and FloPy. Groundwater 2016;54(5):733–9. https://doi.org/10.1111/gwat.12413.

[27] Caljé R. Future use of aquifer thermal energy storage inbelow the historic centre of Amsterdam. (Msc). Delft: Delft University of Technology; 2010.

[28] Possemiers M, Huysmans M, Batelaan O. Application of multiple-point geostatistics to simulate the effect of small-scale aquifer heterogeneity on the efficiency of aquifer thermal energy storage. Hydrogeol J 2015;23(5):971–81. https://doi.org/10.1007/s10040-015-1244-3.

[29] Xynogalou M. Determination of optimal separation well distance for Single Borehole ATES systems in the Netherlands, implementing an axisymmetric numerical model. (MSc). Delft: Delft University of Technology; 2015.

[30] Anderson MP. Heat as a ground water tracer. Ground Water 2005;43(6):951–68. https://doi.org/10.1111/j.1745-6584.2005.00052.x.

[31] Doughty C, Hellstrom G, Tsang CF. A dimensionless approach to the Thermal behaviour of an Aquifer Thermal Energy Storage System. Water Resour Res 1982;18(3):571–87. https://doi.org/10.1029/WR018i003p00571.

[32] Duijff, R. (2019). Interaction between multiple ATES systems. Retrieved from Delft: https://repository.tudelft.nl/islandora/object/uuid%3Acf4bcee3-b775-4676-b683-0e38fabb70ee.

[33] Beernink, S., Hartog, N., Bloemendal, M., & Meer, M. v. d. (2019). ATES systems performance in practice: analysis of operational data from ATES systems in the province of Utrecht, The Netherlands. Paper presented at the European Geothermal Congress, The Hague, Netherlands.

[34] Willemsen, N. (2016). *Rapportage bodemenergiesystemen in Nederland*. Retrieved from Arnhem.

[35] Bloemendal, M., Beernink, S., Bel, N., Hockin, A. E., & Schout, G. (2020). *Transitie open bodemenergiesysteem Koppert-Cress naar verhoogde opslagtemperatuur*. Evaluatie van energiebesparingen en grondwatereffecten. Retrieved from Nieuwegein: https://library.kwrwater.nl/publication/61755396/.

[36] Buday, T. (2014). Reduction of environmental impacts of heat pump usage with special regard on systems with borehole heat exchangers. Landscape & Environment, 8(2). doi:https://ojs.lib.unideb.hu/landsenv/article/view/2310.

[37] Schoots, K., Hekkenberg, M., & Hammingh, P. (2017). *Nationale Energieverkenning 2017*. Retrieved from Petten.

[38] Duijff Rogier, Bloemendal Martin, Bakker Mark. Interaction Effects Between Aquifer Thermal Energy Storage Systems. Groundwater 2021. https://doi.org/10.1111/gwat.13163. In this issue.